Title: Transcriptional Control of Neocortical Size and Microcephaly

Authors: Soraia Barão[1]*, Yijun Xu[1], Rachel Vistein[1], Loyal Goff[1], Kristina Nielsen[1], Byoung-Il Bae[2], Richard S. Smith[3], Christopher A. Walsh[4,5], Genevieve Stein-O'Brien[1]* and Ulrich Müller[1]*

Affiliations:
[1] The Solomon H. Snyder Department of Neuroscience, Johns Hopkins University School of Medicine, Baltimore, MD 21205, USA.
[2] Department of Neuroscience, University of Connecticut School of Medicine, Farmington, CT 06032, USA
[3] Northwestern University, Feinberg School of Medicine, Department of Pharmacology, Chicago, IL, 60611
[4] Division of Genetics and Genomics, Manton Center for Orphan Disease Research, Boston Children's Hospital, Harvard Medical School, Boston, MA 02115, USA
[5] Howard Hughes Medical Institute, Boston Children's Hospital, Harvard Medical School, Boston, MA 02115, USA

*Co-corresponding authors: Ulrich Müller, Soraia Barão and Genevieve Stein-O'Brien. Email: umuelle3@jhmi.edu; sbarao@jhmi.edu; gsteinobrien@jhmi.edu

Abstract:
The mammalian neocortex differs vastly in size and complexity between mammalian species, yet the mechanisms that lead to an increase in brain size during evolution are not known. We show here that two transcription factors coordinate gene expression programs in progenitor cells of the neocortex to regulate their proliferative capacity and neuronal output in order to determine brain size. Comparative studies in mice, ferrets and macaques demonstrate an evolutionary conserved function for these transcription factors to regulate progenitor behaviors across the mammalian clade. Strikingly, the two transcriptional regulators control the expression of large numbers of genes linked to microcephaly suggesting that transcriptional deregulation as an important determinant of the molecular pathogenesis of microcephaly, which is consistent with the finding that genetic manipulation of the two transcription factors leads to severe microcephaly.

Summary:
The neocortex varies in size and complexity among mammals due to the tremendous variability in the number and diversity of neuronal subtypes across species[1,2]. The increased cellular diversity is paralleled by the expansion of the pool of neocortical progenitors[2–5] and the emergence of indirect neurogenesis[6] during brain evolution. The molecular pathways that control these biological processes and are disrupted in neurological and psychiatric disorders remain largely unknown. Here we show that the transcription factors BRN1 (POU3F3) and BRN2 (POU3F2) act as master regulators of the transcriptional programs in progenitors linked to neuronal specification and neocortex expansion. Using genetically modified lissencephalic and gyrencephalic animals, we found that BRN1/2 establish transcriptional programs in neocortical progenitors that control their proliferative capacity and the switch from direct to indirect neurogenesis. Functional studies in genetically modified mice and ferrets show that BRN1/2 act in concert with NOTCH and primary microcephaly genes to regulate progenitor behavior. Analysis of transcriptomics data from genetically modified macaques provides evidence that these molecular pathways are conserved in non-human primates. Our findings thus establish a mechanistic link between BRN1/2 and genes linked to microcephaly and demonstrate that BRN1/2 are central regulators of gene expression programs in neocortical progenitors critical to determine brain size during evolution.

An understanding of cortical progenitor diversity and of the mechanisms by which these progenitors self-renew and differentiate is critical to understand brain evolution and the defects in progenitor behavior that lead to neurological and psychiatric disorders. Cortical progenitors have been broadly divided into two classes named apical progenitors (APs) that undergo mitoses in the ventricular zone (VZ), and basal progenitors (BPs) that undergo mitosis in the subventricular zone (SVZ)[7–11]. APs engage in two modes of neurogenesis termed direct and indirect neurogenesis. During direct neurogenesis, APs divide asymmetrically to self-renew and to generate one neuron, while during indirect neurogenesis, APs divide asymmetrically to self-renew and generate a BP that then gives rise to neurons[7–11]. Indirect neurogenesis generates neurons for all cortical layers but is the predominant neurogenic mode that produces upper layer projection neurons (ULNs)[8,9,12–15]. The number and complexity of ULNs have dramatically increased in gyrencephalic brains, and indirect neurogenesis is thus intricately linked to neocortex expansion during brain evolution[3,5,16,17]. Using *in utero* electroporation and gene targeting in lissencephalic mice and gyrencephalic ferrets as well as single cell transcriptomics analysis in mice and macaques, we reveal here a central function for the POU-homeobox-domain-containing octamer-binding transcription factors BRN1 (POU3F3) and BRN2 (POU3F2) in establishing transcriptional programs that determine the proliferative capacity and neurogenic mode of cortical progenitors to regulate the production of ULNs and thus determine brain size in lissencephalic and gyrencephalic brains. Notably, BRN1 and BRN2 regulate the expression of large numbers of primary microcephaly genes thus implicating transcriptional deregulation as an important determinant of the molecular pathogenesis of microcephaly.

BRN1/2 regulate cell proliferation and the timing of cell cycle exit.
In *Brn1/2-null* mice, the generation of ULNs is severely affected[18,19]. However, effects on brain size could not be evaluated because *Brn1/2-null* mice die at birth when the formation of cortical layers is still in progress. In addition, the molecular and cellular mechanisms by which BRN1/2 regulate neuronal specification are not well understood. Therefore, we generated mice carrying a

floxed *Brn1* allele (*Brn1*^{fl}) and crossed them with mice carrying a floxed *Brn2* allele (*Brn2*^{fl})[20] to generate *Brn1*$^{fl/fl}$*;Brn2*$^{fl/fl}$ mice. We then crossed *Brn1*$^{fl/fl}$*;Brn2*$^{fl/fl}$ mice with *Emx1-Cre* mice[21] on a *Brn1*$^{fl/+}$*;Brn2*$^{fl/+}$ background to generate mice lacking *Brn1/2* in progenitors for excitatory neurons of the dorsal telencephalon (*Brn1/2-cKO* mice) (Extended Data Fig. 1). *Brn1/2-cKO* mice were viable. We confirmed by immunohistochemistry that the expression of BRN1 and BRN2 was efficiently inactivated in the mutant mice already at E12.5 (Extended Data Fig. 1b-d) as expected from the onset of CRE expression in *Emx1-Cre* mice around E10.5[21]. Compared to control littermates, the cortex of *Brn1/2-cKO* mice at postnatal day (P) 13 was reduced in thickness (Fig. 1a,b), had reduced cell numbers (Fig. 1c), and showed abnormal layering with cortical heterotopias (Fig. 1a). Defects in brain size were caused by aberrant generation of ULNs. Accordingly, *Brn1/2-cKO* mice lacked the corpus callosum, which is largely formed by axonal projections of ULNs (Extended Data Fig. 2a,b), and instead had an increased number of subcortical projections (Extended Data Fig. 2c,d). In the somatosensory cortex of *Brn1/2-cKO* mice, the expression of UL markers RORβ and CUX1 was absent with a concomitant increase in the numbers of cells expressing the deep layer (DL) markers TLE4 and CTIP2 (Extended Data Fig. 2e-h). Additionally, the number of glial cells was dramatically increased in in *Brn1/2-cKO* mice at P13 (Extended Data Fig. 3). Consistent with previous studies[18,19], *Brn1* and *Brn2* single homozygous mutants had no obvious defects in cortical development (data not shown).

Prior to gliogenesis, cortical progenitors generate neurons for different cortical layers in sequential order. DL neurons (DLNs) are generated prior to ULNs, which only begin to emerge in mice around E14.5[22]. This temporal order is largely driven by temporal changes in the competence of progenitors to generate distinct neuronal subtypes[23–29]. In addition, some progenitors for ULNs are already present at E12.5 but they begin to differentiate only after E14.5[30–33]. It has been proposed that BRN1/2 in mice are critical to regulate the transition from early- to mid-neurogenesis[18,19,34,35], while BRN2 in monkeys already acts in early progenitors[36]. In contrast to earlier findings, we observed BRN2 expression in murine cortical progenitors already at E11.5 (Extended Data Fig. 1e,f) suggesting that BRN1/2 affects progenitor behavior in mice at earlier time points than previously thought. To test this hypothesis, we inactivated *Brn1/2* using timed *in utero* electroporation (IUE) of pCAG-CRE in *Brn1*$^{fl/fl}$*;Brn2*$^{fl/fl}$ mice at E12.5 and E14.5 (Extended Data Fig. 4a). We co-expressed pCAG-RFP to identify electroporated cells. Relative to controls, BRN1/2-deficient RFP^{+} cells settled in deeper layers regardless of the time point when IUEs were performed (Extended Data Fig. 4b,c,e and f). In addition, experimental manipulations at both ages led to a reduction of BRN1/2-deficient RFP^{+} cells expressing UL markers with a concomitant increase in the number of BRN1/2-deficient RFP^{+} cells expressing DL markers (Extended Data Fig. 4b,d,e and g). These findings suggest that BRN1/2 cell-autonomously regulate the competence of progenitors to generate ULNs starting at early stages of cortical development.

To confirm this hypothesis and to determine the mechanisms by which BRN1/2 regulate neuronal specification, we performed 10X genomics single cell RNA sequencing (scRNAseq) on cortical cells isolated from *Brn1/2-cKO* and wild-type littermates at E12.5 and E14.5 (Fig. 1d). Cells were classified into cell types using cluster analysis and marker gene enrichment (Extended Data Fig. 5a). We then focused our analysis on APs, BPs and excitatory neurons (Fig. 1e,f; Extended Data Fig. 5b-c). In *Brn1/2-cKO* and controls, cell numbers were comparable (Extended Data Fig. 5d) and the proportions of AP cells decreased while the number of BPs and neurons increased between E12.5 to E14.5 (Extended Data Fig. 5d).

Telley et al. (2019) previously reported that APs undergo temporal transcriptional changes (wave 1-6) during their developmental progression[27]. We selected the most reproducible genes representing each transcriptional wave and observed in wild-type mice similar gene expression changes along the pseudotime axis as reported (Fig. 1g-i; Extended Data Fig. 5e; Supplementary Information_1 (SI_1)). In contrast, the transcriptional waves were severely disrupted in APs from *Brn1/2-cKO* mice (Fig. 1i; SI_1). The transcriptional profile of E14.5 *Brn1/2-cKO* APs was more similar to the transcriptional profile of E12.5 control APs with a higher and more prolonged expression of the characteristic E12.5$^{\text{high genes}}$ and a failure to express high levels of the characteristic E14.5$^{\text{high genes}}$ (Fig. 1i; Extended Data Fig. 5f-j; SI_1). We also compared gene expression programs of excitatory neurons from the cortex of control and *Brn1/2-cKO* mice. The expression of UL signature genes was decreased in *Brn1/2-cKO* neurons, while the expression of DL signature genes was increased (Extended Data Fig. 6, SI_2). Gene ontology (GO) terms that significantly changed in *Brn1/2-cKO* neurons included *axon guidance* and *neuron projections* (Extended Data Fig. 6g) consistent with the axonal projection defects that we observed in the mutants at later developmental time points (Extended Data Fig. 2). We conclude that BRN1/2 are critical for the normal regulation of temporal gene expression changes in APs that characterize their progressive restriction in fate potential to progress from the production of DLNs to ULNs.

To further explore the role of *Brn1/2* in progenitor function, we determined the proportion of progenitors in different stages of the cell cycle by analyzing the scRNAseq data using TRIcycle (Transferable Representation and Inference of cell cycle) (Fig. 1j). This method defines cell cycle phase based on the expression of reference genes characteristic for different stages of the cell cycle[37]: (i) G2/M, cells that are preparing to divide (G2) or already have divided (M, mitosis); (ii) S, cells that are synthesizing DNA; (iii) G1/G0, cells that are either waiting to re-enter the cell cycle (G1) or are exiting the cell cycle (G0). The number of progenitors in S-G2/M was reduced in *Brn1/2-cKO* mice and the number of progenitors in G1/G0 was increased (Fig. 1K). The differences were detected at E12.5 but were more pronounced at E14.5. Next, we analyzed cell cycle exit by injecting EdU into pregnant mice at E12.5 and E14.5 and analyzing the number of EdU^{+}/Ki67^{-} cells 24h later (Extended Data Fig. 7a). The number of EdU^{+}/Ki67^{-} cells was significantly increased in *Brn1/2-cKO* mice at E12.5 and E14.5 (Extended Data Fig. 7b). We conclude that in *Brn1/2-cKO* mice, neocortical progenitors are proliferating less and exit the cell cycle faster. Consistent with this phenotype, the expression of numerous cell-cycle associated genes was significantly changed in the *Brn1/2-cKO* progenitors at E12.5 and at E14.5 (Extended Data Fig. 7c,d; SI_3 and SI_4). These genes included *Ezh2* and *Ngn2*, which play important roles at crucial cell cycle transition points[10,38–40]. High levels of *Ezh2* are associated with proliferation of cortical progenitors, while high levels of *Ngn2* are associated with cell cycle exit (Extended Data Fig. 7e)[10,38–40]. The expression of *Ezh2* and *Ngn2* was significantly reduced and increased, respectively, in APs and BPs from *Brn1/2-cKO* mice at E14.5 (Extended Data Fig. 7d,f; SI_3 and SI_4). We confirmed this result by ISH RNAscope for *Ezh2* and *Ngn2* (Extended Data Fig. 7g). In conclusion, in the absence of BRN1/2 the proliferative capacity of progenitors is reduced, and they undergo precocious neurogenesis.

BRN1/2 regulate the balance between direct and indirect neurogenesis via NOTCH signaling.

Since ULNs are absent in *Brn1/2-cKO* mice, we wondered if BRN1/2 might determine the balance between direct and indirect neurogenesis. We combined TRIcycle with the analysis of the expression of *Tbr2* and *MKi67* (Figs. 1j and 2b). *Tbr2* is expressed in IPs and early

differentiating neurons, while *MKi67* specifically labels proliferating cells. *MKi67*$^+$ progenitors are thus actively dividing and among these, *Tbr*2$^+$/*MKi67*$^+$ defines the indirect neurogenesis branch[28]. In contrast, *MKi67*$^-$ cells expressing markers for early differentiation neurons such as *Neurod2* define cells undergoing direct neurogenesis (Fig. 2c)[28]. The proportion of cells going through indirect neurogenesis was significantly decreased in *Brn1/2-cKO* mice at E12.5 and E14.5 (Fig. 2d). These findings were confirmed by TBR2 and Ki67 immunostaining (Fig. 2e) as well as by EdU incorporation analysis in TBR2$^+$ cells (Extended Data Fig. 8a). Since indirect neurogenesis is reduced already at early stages of corticogenesis, we reasoned that the generation of CUX2$^+$ BPs, a subgroup of early generated BPs that is fated to generate ULNs[30,41,42], might be affected in *Brn1/2-cKO* mice. Indeed, the proportion of *Cux2*$^+$ BPs was significantly reduced in *Brn1/2-cKO* mice at E14.5 (Extended Data Fig. 8b-d), a finding that we confirmed by quantifying *Cux2* mRNA expression by ISH RNAscope in TBR2$^+$ cells (Extended Data Fig. 8e). Consistent with the depletion of the CUX2$^+$ BPs fated to generate ULNs in *Brn1/2-cKO* mice, scRNAseq analysis revealed that several UL markers were reduced, while some DL markers were increased in BPs from *Brn1/2-cKO* mice at E14.5 (Extended Data Fig. 8f,f'; SI_4).

Expression levels of HES1 and the NOTCH ligand DLL1 in neural progenitors oscillate with opposite phases, which is critical to regulate the proliferation and differentiation of these cells (Extended Data Fig. 9a)[43,44]. In addition, high levels of *Hes1* and low levels of *Dll1* are associated with direct neurogenesis (Fig. 2a)[6,45]. Since, BRN1/2 suppress the activity of the *Hes1* promoter and cooperate with MASH1 to activate expression of *Dll1*[34,46], we wondered whether defects in *Hes1* and *Dll1* expression might explain the defects in indirect neurogenesis in *Brn1/2-cKO* mice. scRNAseq analysis revealed that *Hes1* was dramatically overexpressed in *Brn1/2-cKO* progenitors at E14.5 (Fig. 2f; SI_5). In contrast, expression of *Notch1* and *Dll1* were significantly reduced (Fig. 2f; SI_5). We confirmed these findings by ISH RNAscope (Extended Data Fig. 9b). Given the cross-regulatory interactions between HES1 and DLL1[43,44], we expected that the amplitude of oscillatory gene expression of NOTCH signaling pathway components might be affected in *Brn1/2-cKO* mice. We analyzed EdU incorporation and the expression of HES1 during cell cycle in control and *Brn1/2-cKO* mice 90 minutes (90'; S+G2 phase), 8h (early G1) or 14h (late G1) after EdU injection into pregnant mice at E14.5 (Extended Data Fig. 9c). Although the typical HES1 oscillations still occurred in *Brn1/2-cKO* progenitors (Extended Data Fig. 9c), levels of HES1 were vastly increased compared to controls at any time during the cell cycle (Fig. 2g; Extended Data Fig. 9c). Even lowest levels of HES1 in mutants never fell below highest levels in controls (Fig. 2g; Extended Data Fig. 9c). We conclude that BRN1/2 play a crucial role in establishing normal expression patterns of NOTCH signaling pathway components in progenitors.

To provide direct evidence for a causal relationship between perturbations in NOTCH signaling and the changes in indirect neurogenesis in *Brn1/2-cKO* mice, we inactivated *Brn1/2* by IUE of *Brn1*$^{fl/fl}$;*Brn2*$^{fl/fl}$ mice at E14.5 using pCAG-CRE and analyzed neurogenesis at E16.5 (Fig. 2h). We co-expressed pCAG-RFP to identify electroporated cells. The number of mutant RFP$^+$ cells going through indirect neurogenesis was significantly reduced (Fig. 2i,k), while the number of mutant RFP$^+$/NEUROD2$^+$ cells was significantly increased consistent with a higher rate of direct neurogenesis (Fig. 2j,k). We next co-expressed pCAG-CRE to inactivate *Brn1/2* and pCS2-NOTCH1 to overexpress NOTCH1. While NOTCH1 overexpression did not change the rate of indirect neurogenesis (RFP$^+$/TBR2$^+$ cells) and neuronal production (RFP$^+$/NEUROD2$^+$ cells) in wild-type (Extended Data Fig. 9d-f), it restored levels of indirect neurogenesis and neuronal production in the *Brn1/2-cKO* condition to control levels (Fig. 2i-k).

Significantly, overexpression of DLL1 in *Brn1*$^{fl/fl}$*;Brn2*$^{fl/fl}$ mice phenocopied the effect of NOTCH1 overexpression (Fig. 2l; Extended Data Fig. 9g-i), which is consistent with the idea that an imbalance in DLL1-dependent NOTCH1 signaling in progenitors is responsible for the defects in indirect neurogenesis in *Brn1/2-cKO* mice (Fig. 2a).

BRN1/2 are required to maintain the neuronal progenitor pool through the regulation of microcephaly-associated genes.

Increases in brain size during evolution are accompanied by a disproportionate increase in ULNs compared to DLNs, and the production of ULNs is frequently affected in microcephaly patients[17]. Because ULNs are massively affected by defects in BRN1/2 function and the brain of *Brn1/2-cKO* mice is vastly more microcephalic than is typical for most microcephaly mouse models, we wondered whether BRN1/2 are required for the expression and function of sets of genes linked to microcephaly. ScRNAseq analysis revealed that the expression of a large number of genes that when mutated cause microcephaly in humans was significantly decreased in *Brn1/2-cKO* progenitors (Fig. 3a; SI_5). These included 11 classical primary microcephaly genes: *Cdk5rap2* (MCPH3), *Knl1* (MCPH4), *Aspm* (MCPH5), *Cenpj* (MCPH6), *Stil* (MCPH7), *Cep135* (MCPH8), *Cdk6* (MCPH12), *Sass6* (MCPH14), *Mfsd2a* (MCPH15), *Cit* (MCPH17) and *Copb2* (MCPH19)[47]. We confirmed these findings for *Aspm* and *Cdk6* by ISH RNAscope at E14.5 (Extended Data Fig. 10a).

Knock-out of *ASPM* in ferret, a small carnivore characterized by an expanded and gyrencephalic neocortex, phenocopies the microcephaly defect in human patients[48]. We therefore compared the cortical phenotype of *Brn1/2-cKO* mice and *ASPM*KO ferrets. In *ASPM*KO ferrets, APs detached prematurely from the VZ resulting in increased number of terminal divisions and premature differentiation towards the glial lineage (Fig. 3b-e; Extended Data Fig. 10d-f')[48]. APs in *Brn1/2-cKO* mice were similarly displaced at E14.5 (Fig. 3f,f',g) and the number of glial cells was also increased at P0 (Fig. 3h,h'). In addition, the number of neuronal progenitors declined more rapidly throughout embryonic development in *Brn1/2-cKO* mice compared to controls (Fig. 3i; Extended Data Fig. 10b) and glial numbers were further increased at P13 (Extended Data Fig. 3). Although the neocortical distribution of TBR2^{+}Ki67^{+} cells is also increased outside of the VZ (Extended Data Fig. 10g), the balance between direct and indirect neurogenesis is not affected in *ASPM*KO ferrets at E35 (Extended Data Fig. 10h). *ASPM*KO thus phenocopies aspects of the phenotype in *Brn1/2-cKO* mice, consistent with the model that *ASPM* expression is regulated by *Brn1/2*.

Since *Aspm* and most of the microcephaly-associated genes altered in *Brn1/2-cKO* progenitors encode centrosome proteins[47], we tested how the absence of BRN1/2 affects centrosome function in progenitors. The expression of genes essential for centrosome function were significantly reduced in *Brn1/2-cKO* progenitors at E14.5 (Extended Data Fig. 10c; SI_5) and centriole duplication was disrupted (Fig. 3j) suggesting that defects in *ASPM* expression, and possibly in other microcephaly genes, contribute to the cortical phenotype of *Brn1/2-cKO* mice (Fig. 3k).

BRN1/2 function is conserved across phylogeny.

In *BRN2*KO monkeys, the neurogenic behavior of cortical progenitors is similarly altered as in *Brn1/2-cKO* mice[36]. To test if the mechanisms by which BRN1/2 regulate progenitor behavior are evolutionary conserved, we first inhibited BRN1/2 activity in wild-type ferrets at E35 by IUE with pCAG-*Brn*-DBD-EnR, a dominant negative inhibitor of BRN1/2 function (Fig. 4a)[34,46]. 48h

after *Brn*-DBD-EnR expression, the number of dividing progenitors ($RFP^+/Ki67^+$) was significantly reduced, indicative of faster cell cycle exit compared to controls (Fig. 4b,e). The number of cells going through indirect neurogenesis ($RFP^+/TBR2^+$) was significantly reduced (Fig. 4c,e), while neuronal output ($RFP^+/NEUROD2^+$ cells) was increased (Fig. 4d,e). Additionally, the expression of *Notch1* was reduced in the cortex of ferrets expressing *Brn*-DBD-EnR (Fig. 4f-f'). Thus, our results in ferrets mirror those in mice, providing evidence for a conserved role for BRN1/2 in cortical progenitors of lissencephalic and gyrencephalic brains. In further support of this hypothesis, in the cortex of ferrets expressing *Brn*-DBD-EnR the expression of *Aspm* and *Cdk6* was also reduced (Fig. 4g), resulting in an increase of $RFP^+/OLIG2^+$ cells and total $OLIG2^+$ cells (Fig. 4h,h').

Next, we analyzed available raw scRNAseq data from *BRN2*KO monkeys at E36[36] using identical criteria as employed in our analysis of scRNAseq from mice (Fig. 4i-k). We identified APs, BPs and neurons (Fig. 4l) and used the BP gene expression signature, the expression profile of *MKi67* and TRIcycle analysis (Fig. 4m1-3), to identify cells going through direct and indirect neurogenesis (Fig. 4n). Similar to our findings in mice, the proportion of cells going through indirect neurogenesis was significantly reduced in *BRN2*KO monkeys (Fig. 4o). Expression of *NOTCH1* was reduced while *HES1* was dramatically increased in *BRN2*KO progenitors (Fig. 4p; SI_6). Unlike in mice, *DLL1* expression was increased in *BRN2*KO progenitors (Fig. 4p; SI_6). Effects on the expression of *DLL1* might not be observed in monkeys because BRN1 may compensate in part for loss of BRN2. Alternatively, the regulation of NOTCH signaling pathways in monkeys might reflect differences between species. Interestingly, the expression of some UL markers was already reduced in the *BRN2*KO neurons at E36 (Fig. 4q; SI_6). In addition, the expression of 9 classical microcephaly genes (*MCPH1*, *CDK5RAP2* (MCPH3), *ASPM* (MCPH5), *CENPJ* (MCPH6), *STIL* (MCPH7), *CEP135* (MCPH8), *SASS6* (MCPH14), *CIT* (MCPH17) and *WDFY3* (MCPH18))[47] was reduced in *BRN2*KO progenitors at E36 (Fig. 4r; SI_6) mimicking the results in *Brn1/2-cKO* mice.

Overall, our findings reveal a striking similarity in the defects caused by perturbations in BRN1/2 function in mice, ferrets and monkeys, supporting a model in which BRN1/2 have evolutionarily conserved functions to regulate neocortical progenitor behavior in lissencephalic and gyrencephalic animals.

Discussion

The molecular mechanisms that regulate the behavior of cortical progenitors in the mammalian clade and thus control brain size are not well understood. We show here that BRN1/2 are key drivers of the transcriptional programs in neocortical progenitors of mice, ferrets and monkeys that determine the timing of their differentiation and their total output of ULNs. Loss of BRN1/2 in progenitors leads to the deregulation of the expression of genes that regulate cell cycle progression, NOTCH signaling and centrosome function, thus coordinating the expression of sets of genes that affect different aspects of progenitor behavior. Our functional studies demonstrate that deregulation of NOTCH signaling contributes to defects in indirect neurogenesis and the production of ULNs, which is consistent with previous studies demonstrating the crucial function of NOTCH signaling for regulating the neurogenic mode of cortical progenitors[6,45]. Defects in centrosome function are likely caused by deregulation of the expression of microcephaly genes as shown by perturbation of ASPM function[48]. Centrosomes have crucial roles in the organization of microtubules and regulate cell polarity, the formation of primary cilia and mitotic spindle assembly[49]. Defects in centrosome function likely result in precocious cell cycle exit in

Brn1/2-cKO progenitors and accelerated depletion of neuronal progenitors during progressive stages of neurogenesis, contributing to the absence of ULNs, increased gliogenesis and reduced brain size.

While our findings provide evidence for an evolutionary conserved role for BRN1/2 regulation of transcriptional programs that control progenitor behavior, it remains to be established to what extent the function of these transcriptional regulators has been modified during brain evolution to produce differences in brain size. For example, disruption of BRN2 function alone affects cortical development in monkeys[36], but not in mice[18,19], suggesting that redundancy of BRN1 and BRN2 function is not universally conserved. In addition, recent studies have shown that during evolution, enhancers that control neuronal gene expression have been altered by mutations that affect predominantly binding sites for a limited set of transcription factors, including BRN1/2[50]. Microcephaly associated genes are included in the list of genes that contain enhancer elements enriched in BRN1/2 binding sites[50]. Changes to regulatory regions of the genome that affect the transcriptional landscape are thus likely to be intricately linked to adaptive changes crucial for neocortical expansion and affected in microcephaly in humans.

Methods:

Mice

All animal experiments adhered to the guidelines of the National Institute of Health and were approved by the Institutional Animal Care and Use Committee at Johns Hopkins University School of Medicine. Mice were maintained on a 14h light/10h dark cycle. Both male and female mice were used, and no obvious differences between the sexes were noted. All mice were group-housed in pathogen-free facilities with regulated temperature and humidity and given *ad libitum* access to food and water. All mice used were seemingly free of infection, health abnormalities or immune system deficiencies and were employed independently of their gender. None of the mice used had been used for previous experiments. The date of the vaginal plug detection was designated E0.5, and the date of birth P0. *Emx1-Cre* [B6.129S2-*Emx1tm1(cre)Krj*][21] and *Brn2* conditional knockout [*Brn-2*$^{fl/fl}$][20] mice have been described. *Brn1* conditional knockout mouse was generated in collaboration with Janelia Research Campus - Howard Hughes Medical Institute. The embryonic stem cells (ESCs) were designed to insert loxP sites flanking the coding sequence of *Brn1* gene, with upstream elements including a neomycin-resistance cassette (PGK-neo) and *lacZ* reporter flanked by two FRT sites. ESCs were transplanted into mouse blastocysts to produce transgenic mice. Heterozygous F1 mice (*Brn1flox-neo/+*) were mated with *FLPe* mice to remove the PGK-neo cassette and *lacZ* reporter. The resulting offspring were subsequently mated to C57BL/6J mice to remove the *FLPe* transgene. C57BL/6J wild type mice were obtained from Charles River Laboratories. *Brn1*$^{fl/fl}$ and *Brn2*$^{fl/fl}$ mice were crossed and the resulting *Brn1*$^{fl/fl}$*;Brn2*$^{fl/fl}$ mice were crossed with heterozygous *Emx1-Cre* mice. Animals with no CRE-recombination were used as control littermates in the scRNAseq experiments. Animals with no CRE-recombination or heterozygous for one or the two genes (*Brn1* and *Brn2*) were used as control littermates in the different histological experiments. We used these mice interchangeably because they were indistinguishable from each other and from wild-type mice.

Ferrets

All procedures adhered to the guidelines of the National Institute of Health and were approved by the Animal Care and Use Committee at Johns Hopkins University. Experiments were performed in female ferrets (*Mustela putoris furo*, Marshall BioResources) with normal immune status. Animals were housed in a 16h light/8h dark cycle. Ferrets were not involved in previous studies. The *ASPM*KO brain sections[48] were obtained through the collaboration with Dr. Byoung-Il Bae, Dr. Richard S. Smith and Dr. Christopher A. Walsh.

Immunohistochemistry

Embryonic brains were fixed in 4% paraformaldehyde (PFA) in phosphate-buffered saline (PBS) for 2-4h at 4°C. Postnatal mice were transcardially perfused with 20 ml ice-cold 4% PFA using a peristaltic pump at a rate of 2 ml/min. Brains were removed from the skull and postfixed in 4% PFA overnight at 4°C. Embryonic brains were cryopreserved with 30% sucrose, embedded in Tissue-Tek O.C.T. compound (#4583, SAKURA) and frozen at -80°C. They were then sectioned coronally at 16 µm with a cryostat (CM3050 S, Leica). Postnatal brains were embedded in 3% low melting point agarose (#R0801, Thermo Fisher Scientific) in PBS and sectioned coronally or sagittally at 60 µm with a vibrating microtome (VT1200S, Leica). For immunohistochemistry, brain sections were permeabilized in PBS containing 0.2% Triton X-100 and blocked in 10% goat serum for 1h at room temperature. Brain slices were then incubated with primary antibodies in blocking solution overnight (or 48h depending on the thickness of the section and antibody

used) at 4°C and subsequently incubated with the appropriate secondary antibodies diluted in blocking solution for 2h at room temperature. To label all cell nuclei, the fluorescent nuclear dye DAPI (1 μg/ml, #D9542, Sigma-Aldrich) was included with the secondary antibody solution. The sections were mounted with ProLong™ Gold (#P36930, Thermo Fisher Scientific). Primary antibodies used were: anti-L1 (1:500, rat monoclonal, MAB5272 Millipore Sigma); anti-TLE4 (1:500, rabbit polyclonal, ab64833 Abcam); anti-CTIP2 (1:1000, rat monoclonal, ab18465 Abcam); anti-RORβ (1:500, mouse monoclonal, PP-N7927-00 R&D systems); anti-CUX1 (1:1000, rabbit polyclonal, 11733-1-AP Proteintech); anti-GFP (1:500, chicken polyclonal, GFP-1020 Aves Labs Inc.); anti-BRN2 (1:1000, rabbit polyclonal, PA5-30124 Thermo Fisher Scientific or 1:1000, rabbit monoclonal, 12137 Cell Signaling); anti-BRN1 (1:1000, rabbit polyclonal, sc-6028-R Santa Cruz Biotechnology); anti-NeuN (1:500, mouse monoclonal, MAB377 Millipore Sigma); anti-Ki67 (1:500, rabbit polyclonal, ab15580 Abcam or 1:500, rat monoclonal, 14-5698-82 Thermo Fisher Scientific); anti-RFP (1:1000, rat monoclonal, 5F8 ChromoTek or 1:1000, rabbit polyclonal, ab62341 Abcam); anti-Pax6 (1:250, mouse monoclonal, MA1-109 Thermo Fisher Scientific); anti-TBR2 (1:500, rat monoclonal, 14-4875-82 Thermo Fisher Scientific or 1:500, rabbit polyclonal, ab183991 Abcam); anti-NEUROD2 (1:500, rabbit polyclonal, ab104430 Abcam); anti-HES1 (1:1000, rabbit polyclonal, R. Kageyama gift[43]); anti-pVIM (1:500, mouse monoclonal, D076-3 MBL); anti-OLIG2 (1:500, rabbit polyclonal, AB9610 Millipore Sigma); anti-SOX9 (1:1000, rabbit monoclonal, ab185966 Abcam); anti-GFAP (1:1000, chicken polyclonal, AB5541 Millipore Sigma); anti-PH3 (1:1000, rat monoclonal, ab10543 Abcam); anti-γ-TUBULIN (1:500, goat polyclonal, A. Holland gift[51]); anti-Centrin (1:500, rabbit polyclonal, A. Holland gift[52]). Secondary antibodies used were: Alexa 555, 647, 488 anti-rat (A21434; A21247, A11006), anti-rabbit (A21430; A21246) and anti-mouse (A21425; A21237); Alexa 488 anti-rabbit (A11070); Alexa 488 and 647 anti-chicken (A11039; A21449); anti-rabbit HRP (A27036); all diluted 1:500 and all from Thermo Fisher Scientific. Antigen retrieval[53] was performed for all immunohistochemistry at embryonic ages and to stain for OLIG2 and RORβ postnatally. The method used here was a heat-induced citrate method[53]. HES1 immunostaining was done using a horseradish peroxidase (HRP)-secondary antibody and an additional tyramide signal amplification (TSA) step. Therefore, after antigen retrieval, the brains sections were treated with 3% hydrogen peroxide to block HRP-unspecific binding. After the secondary antibody, the sections were washed and incubated with TSA solution (#NEL744001KT, Akoya Biosciences) overnight at 4°C. The sections were then mounted with ProLong™ Gold.

RNAscope multiplex *in situ* hybridization

Brain sections were processed for multiplex fluorescent *in situ* hybridization RNAscope[54] following the manufacturer's instructions (#323110, Advanced Cell Diagnostics). Gene-specific probes: *Fezf2(*313301-C2), *Satb2(*413261), *Ezh2(*446611-C2), *Ngn2 (*417291-C2), *Cux2* (469551-C3), *Notch1(*404641), *Dll1(*425071-C2), *Hes1(*417701), *Aspm (*427881) *and Cdk6 (*570091-C2). When we combined RNAscope with immunohistochemistry, the sections were briefly washed in 1X PBS after the last conjugation step and the immunohistochemistry protocol was followed as previously described.

EdU injections and labeling

EdU (5-ethynyl-2´-deoxyuridine; #A10044, Thermo Fisher Scientific) was diluted at 10mg/ml in 0.9% NaCl (#114-055-101, Quality Biological) and administered in pregnant females at the

specified embryonic pregnancy stage at 50mg/Kg body weight. For proliferation analysis, a single intraperitoneal EdU injection was administered at E12.5 or E14.5, embryos were fixed after 1h and the number of EdU^+ cells quantified. For cell cycle exit calculation, a single intraperitoneal EdU injection was administered at E12.5 or E14.5, embryos were fixed after 24h and the percentage of EdU^+ cells labeled with Ki67 was calculated. For HES1 expression analysis during different phases of cell cycle, EdU was injected at E14.5, embryos were fixed after 90 min (S+G2), 8h (early G1) or 14h (late G1) and the percentage of EdU^+ cells labeled with HES1 was calculated. EdU was labeled using Click-iT® EdU imaging kits with alexa 555 or 647 following the manufacturer's instructions (#C10638 or #C10340, Thermo Fisher Scientific). Briefly, brain sections were post-fixed with 3.7% formaldehyde and permeabilized with 0.5% Triton X-100 in PBS. The Click-iT® reaction cocktail was then added, and the sections incubated in the dark for 30 minutes at room temperature. After the washes, the brain sections were stained for the different proteins of interest using the immunohistochemistry protocol previously described.

Expression Constructs

pCAG-mRFP (plasmid #32600, Addgene) was deposited by Anna-Katerina Hadjantonakis[55]. pCAG-CRE (plasmid #13775, Addgene) was generated by Connie Cepko[56]. pCS2 NOTCH1 Full Length-6MT (pCS2-*Notch1-FL*, plasmid #41728, Addgene) was deposited by Raphael Kopan[57]. pCAG-Brn-DBD-EnR (plasmid #19714, Addgene) was generated by Connie Cepko[58]. pCMV6 Delta1 Full Length Myc-DDK was obtained from Origene (pCMV6-*Dll1-FL*, #MR226161).

***In utero* electroporation in mice**

The protocol used here was adapted from Saito and Nakatsuji[59]. For electroporation of embryonic day 12.5 (E12.5) embryos, five 50 ms pulses of 30 V were delivered (E14.5 – 80ms, 40V). Embryos were left to develop *in utero* for the indicated time or females were allowed to give birth and pups were euthanized at the indicated age.

***In utero* electroporation in ferrets**

The protocol used here followed the established method described by Kawasaki et al.[60]. Briefly, pregnant ferrets were anesthetized with ketamine, and their body temperature was monitored and maintained using a bair hugger warmer. Anesthesia was then continued with isoflurane at 1-2%. Respiratory rate was closely observed, and analgesic solution was injected subcutaneously (Buprenorphine, 0.001 mg/Kg). For E35 electroporation five 50 ms pulses of 100 V were delivered. The embryos were left to develop *in utero* for 48h.

Single cell RNA sequencing

Tissue preparation and single cell RNA sequencing: Cortex of E12.5 and E14.5 embryos was dissected and dissociated into single cells using the Papain Dissociation System (#LK0031500, Worthington Biochemical). Individual collected cells were processed for scRNAseq using. Cell counts and viability were determined using the Cell Countess II with Trypan Blue. A maximum volume of 43.3 µl/sample was used for processing to target up to 10,000 cells. Cells were combined with RT reagents and loaded onto 10X Next GEM Chip G along with 3' v3.1 gel beads. The NextGEM protocol was run on the 10X Chromium Controller to create GEMs, composed of a single cell, gel bead with unique barcode and UMI primer, and RT reagents. 100 µl of emulsion is retrieved from the chip and incubated (45 min at 53°C, 5 min at 85°C, cool to

4°C), generating barcoded cDNA from each cell. The GEMs were broken using Recovery Agent and cDNA cleaned, following manufacturer's instructions using MyOne SILANE beads. cDNA was amplified for 11 cycles (3 min at 98°C, 11 cycle: 15 sec at 98°C, 20 sec at 63°C, 1 min at 72°C; 1 min at 72°C, cool to 4°C). Samples were cleaned using 0.6X SPRIselect beads. Quality control (QC) was completed using Qubit and Bioanalyzer to determine size and concentrations. 10 µl of amplified cDNA was carried into library prep. Fragmentation, end repair and A-tailing were completed (5 min at 32°C, 30 min at 65°C, cool to 4°C), and samples were cleaned up using double sided size selection (0.6X, 0.8X) with SPRIselect beads. Adaptor ligation (15 min at 20°C, cool to 4°C), 0.8X cleanup and amplification were performed by PCR using unique i7 index sequences. Libraries underwent a final cleanup using double sided size selection (0.6X, 0.8X) with SPRIselect beads. Library QC was performed using Qubit, Bioanalyzer and KAPA library quantification qPCR kit. Libraries were sequenced on the Illumina NovaSeq 6000 using v1.5 kits, targeting 50K reads/cell, at read lengths of 28 (R1), 8 (i7), 91 (R2). Demultiplexing and FASTQ generation was completed using Illumina's BaseSpace software. Data were aligned to the mouse reference genome (refdata-gex-mm10-2020-A) publicly available at the 10X genomics' website using the Cell Ranger pipeline. Although we started with seven *Brn1/2-cKO* and seven wild-type littermates of both sexes the genotype for one of the wild-type samples could not be confirmed and therefore this sample was removed from the analysis.

Single cell RNA sequencing analysis: Briefly, the 10x data were manually aggregated to create a comprehensive data set and subjected to additional QCing. Raw counts were aggregated together for input into the Monocle3 R/Bioconductor platform and preprocessing performed as previously described[61]. Batch correction was done using the aligned_cds function within Monocle3 for the purpose of visualization[62]. Dimensionality reduction and visualization for the aggregate 10x data were performed using Uniform Manifold Approximation and Projection (UMAP)[63] for all cells passing QC. Briefly the first 50 principle components of the log10(CPT+1) was used as input for the monocle3 implementation of the UMAP algorithm with the following additional parameters: max_components = 3, metric = ''cosine''. Initial cell clusters were called using the louvain algorithm with manual annotation using marker genes. The progenitor and neuronal lineages were subset from the main data using this initial clustering. A new embedding was learned for this subset and cell with ambiguous identity were removed. Although we sequenced seven *Brn1/2-cKO* and seven wild-type littermates of both sexes (total cells = 161,000) the genotype for one of the wild-type samples could not be confirmed and therefore this sample was removed from the subsequent analysis (total cells = 149,712). AP (28% of cells), BP (6.7% of cells), Neurons (31% of cells), DL and UL signatures scores were calculated using the AddModuleScore function from Seurat with cell type signatures from Telley et al.[26,27] and refined the combination of the results of the clustering and the module Scores with additional marker genes[26–29,64].TRIcycle analysis was performed as previously described[37]. Final cell types were called using a combination of cluster analysis and cell marker genes[26–29]. All differential expression tests were performed across all expressed genes using the Monocle3 VGAM likelihood ratio test with batch and conditions included in the model formula[61]. Additional statistical tests were carried out in R/Bioconductor. Unpaired t-test was used to compare the total cell types per age and genotype. Wilcoxon rank sum test was used for TRIcycle cell cycle phase analysis and Pearson's Chi-squared test for given probabilities was used for cell proportion analysis. The heatmaps and dotplots were generated with ggplot2 using the row normalized nonzero means. The DE genes were selected using the following thresholds: standard error < 0.15, q value ≤ 0.001 for neurons, AP and BP, and q value ≤ 0.05 for all

progenitors (AP and BP together). The ribosomal and mitochondrial genes were removed. GO analysis was performed by the Enrichr API from Gseapy using the filtered DE lists. The terms of interest were selected for visualization from the significant terms with adjusted q value less than 0.05. The embedding of cynomolgus monkey data was generated by scanpy. Cells with less than 5500 UMIs were excluded. The UMAP was generated with the first 15 principle components and the min_dist of 0.3. AP, BP, UL, and DL signatures scores were calculated using the "score_genes" function. The TRIcycle and DE gene analysis used the same setting as described above. The DE genes were selected by the following criteria: standard error $\leq$ 0.15, q value $\leq$ 0.001 for neurons and q value $\leq$ 0.05 for all progenitors (AP and BP together).

Transcriptional waves along pseudotime projection: Only AP cells were selected to learn the pseudotime projection for cell maturity. First, we performed the dimensionality reduction on the control cells. Since one of the sequencing batches (Batch 1) failed to show temporal difference in the latent space, we removed this batch from the following pseudotime analysis. In the latent space of the remaining control data, the second and third principal components best describe the temporal difference and explain a significant amount of variance. Therefore, we fitted a principal curve based on these two PCs using prinPY and projected the cells back into the fitted trajectory to define the maturity pseudotime. The side with highest expression of *Sox2* and *Hmga2* was selected as the beginning as previously described[27] and the pseudotime score was normalized between 0 to 1. For the *Brn1/2-cKO* cells, we used KDtree to search for their nearest neighbor among control cells in the latent space and assigned the *Brn1/2-cKO* cells with the same pseudotime score as its nearest control neighbor. We then visualized the previously described temporal wave genes using Seaborn heatmap. The cells were aligned according to their pseudotime score and the heatmap was smoothed by the UnivariateSpline. We have confirmed that the control and *Brn1/2-cKO* cells from Batch 1 showed similar average age-related expression pattern compared with the other batches within the same genotype for the vast majority of the genes used to define the transcriptional waves.

Imaging

All immunohistochemistry and ISH RNAscope data were acquired in an equivalent latero-medial level of the cortex from at least 3 independent animals per condition or genotype. Images were captured using a Zeiss LSM 800 confocal microscope. Maximum intensity projections were generated in ImageJ or Imaris software. In all fluorescence microscopy figures, different channels of image series were represented in pseudocolor, and contrast and brightness were adjusted manually using ImageJ or Adobe Photoshop software. All markers were counterstained with DAPI to allow visualization of overall cellular density.

Histological analysis

A series of *z*-stack (depth of 10 μm) confocal tiled images were used for cell quantification; 150 μm-wide images (embryonic brains) or 300 μm-wide images (postnatal brains) comprising the entire extension of the cortex were analyzed. All quantification were made in an equivalent latero-medial level of the cortex from at least 3 independent animals per condition or genotype. The number of cells expressing the markers of interest was quantified in a radial section of the same latero-medial level and adjusted per area. For the IUE analysis, to divide the cortex into longitudinal bins, a rectangle was drawn from the border of the white matter with layer VI to the pial surface. This rectangle was then divided into ten equal bins and the number of cells within each bin was quantified. To quantify ISH-RNAscope data, all punctate dots or all punctate dots

in RFP^+ cells were counted in 50 µm-wide images comprising the entire extension of the cortex. *Notch1* mRNA levels in the ferret *in utero* electroporated cells were quantified in all RFP^+ cells in the area comprising 50 µm from the VZ. For the centriole number analysis, a z-stack of 10 sections (0.5µm each) was selected for all analyzed cells and the number of centrioles overlapping or in the very close proximity of the g-TUBULIN staining were counted. Since *Brn1/2-cKO* show a 20% reduction of total cell number and cortical thickness, the quantifications were normalized to the cortical thickness of each analyzed section in controls and mutants.

Statistical analysis

Statistical analyses of the immunohistochemistry and ISH-RNAscope experiments were done using GraphPad Prism software. Statistically significant differences were assessed by Student's unpaired t-test or one-way analysis of variance (one-way ANOVA – Dunnett's multiple comparisons test; $F_{DFn,\ DFd}$ (DFn: degrees of freedom in the numerator; DFd: degrees of freedom in the denominator)), comparing two or more groups, respectively. To compare the distribution of RFP^+ cells in the different bins of the cortex for the two different conditions we used two-way analysis of variance (two-way ANOVA – Šídák's multiple comparisons test; $F_{DFn,\ DFd}$). $P<0.05$ was considered a significant difference. All values represent individual animals mean ± standard error of the mean (SEM). The statistical test used, and the statistical significance are indicated in figure legends. Statistical analyses of the scRNAseq experiments were done using Monocle 3 and R/Bioconductor. Monocle3 VGAM likelihood ratio test was used for the differential expressed gene analysis. Unpaired t-test was used to compare the total cell types per age and genotype. Wilcoxon rank sum test was used for TRIcycle cell cycle phase analysis and Pearson's Chi-squared test for given probabilities was used for cell proportion analysis.

References:

1. Lodato, S. & Arlotta, P. Generating Neuronal Diversity in the Mammalian Cerebral Cortex. *Annu. Rev. Cell Dev. Biol* **31**, 699–720 (2015).
2. Borrell, V. & Reillo, I. Emerging roles of neural stem cells in cerebral cortex development and evolution. *Dev Neurobiol* **72**, 955–971 (2012).
3. Kalebic, N. & Huttner, W. B. Basal Progenitor Morphology and Neocortex Evolution. *Trends Neurosci* **43**, 843–853 (2020).
4. Pinson, A. & Huttner, W. B. Neocortex expansion in development and evolution—from genes to progenitor cell biology. *Curr Opin Cell Biol* **73**, 9–18 (2021).
5. Pebworth, M. P., Ross, J., Andrews, M., Bhaduri, A. & Kriegstein, A. R. Human intermediate progenitor diversity during cortical development. *Proc Natl Acad Sci U S A* **118**, 1–10 (2021).
6. Cárdenas, A. *et al.* Evolution of Cortical Neurogenesis in Amniotes Controlled by Robo Signaling Levels. *Cell* **174**, 590-606.e21 (2018).
7. Noctor, S. C., Flint, A. C., Weissman, T. A., Dammerman, R. S. & Kriegstein, A. R. Neurons derived from radial glial cells establish radial units in neocortex. *Nature* **409**, 714–720 (2001).
8. Haubensak, W., Attardo, A., Denk, W. & Huttner, W. B. Neurons arise in the basal neuroepithelium of the early mammalian telencephalon: A major site of neurogenesis. *Proc Natl Acad Sci U S A* **101**, 3196–3201 (2004).
9. Noctor, S. C., Martínez-Cerdeño, V., Ivic, L. & Kriegstein, A. R. Cortical neurons arise in symmetric and asymmetric division zones and migrate through specific phases. *Nat Neurosci* **7**, 136–44 (2004).
10. Miyata, T. *et al.* Asymmetric production of surface-dividing and non-surface-dividing cortical progenitor cells. *Development* **131**, 3133–3145 (2004).
11. Hansen, D. V., Lui, J. H., Parker, P. R. L. & Kriegstein, A. R. Neurogenic radial glia in the outer subventricular zone of human neocortex. *Nature* **464**, 554–561 (2010).
12. Tarabykin, V., Stoykova, A., Usman, N. & Gruss, P. Cortical upper layer neurons derive from the subventricular zone as indicated by Svet1 gene expression. *Development* **128**, 1983–1993 (2001).
13. Kowalczyk, T. *et al.* Intermediate neuronal progenitors (basal progenitors) produce pyramidal-projection neurons for all layers of cerebral cortex. *Cerebral Cortex* **19**, 2439–2450 (2009).
14. Vasistha, N. A. *et al.* Cortical and clonal contribution of Tbr2 expressing progenitors in the developing mouse brain. *Cerebral Cortex* **25**, 3290–3302 (2015).
15. Huilgol, D. *et al.* Direct and indirect neurogenesis generate a mosaic of distinct glutamatergic projection neuron types in cerebral cortex. *Neuron* **111**, 2557-2569.e4 (2023).
16. Reillo, I., De Juan Romero, C., García-Cabezas, M. Á. & Borrell, V. A Role for intermediate radial glia in the tangential expansion of the mammalian cerebral cortex. *Cerebral Cortex* **21**, 1674–1694 (2011).
17. Molnár, Z. *et al.* New insights into the development of the human cerebral cortex. *J Anat* **235**, 432–451 (2019).
18. McEvilly, R. J., Ortiz de Diaz, M., Schonemann, M. D., Hooshmand, F. & Rosenfeld, M. G. Transcriptional regulation of cortical neuron migration by POU domain factors. *Science* **295**, 1528–1532 (2002).

19. Sugitani, Y. *et al.* Brn-1 and Brn-2 share crucial roles in the production and positioning of mouse neocortical neurons. *Genes Dev* **16**, 1760–1765 (2002).
20. Jaegle, M. *et al.* The POU proteins Brn-2 and Oct-6 share important functions in Schwann cell development. *Genes Dev* **17**, 1380–91 (2003).
21. Gorski, J. A. *et al.* Cortical excitatory neurons and glia, but not GABAergic neurons, are produced in the Emx1-expressing lineage. *J Neurosci* **22**, 6309–14 (2002).
22. Greig, L. C., Woodworth, M. B., Galazo, M. J., Padmanabhan, H. & Macklis, J. D. Molecular logic of neocortical projection neuron specification, development and diversity. *Nat Rev Neurosci* **14**, 755–769 (2013).
23. McConnell, S. K. & Kaznowski, C. E. Cell cycle dependence of laminar determination in developing neocortex. *Science* **254**, 282–285 (1991).
24. Frantz, G. D. *et al.* Restriction of Late Cerebral Cortical Progenitors to an Upper-Layer Fate. *Neuron* **17**, 55–61 (1996).
25. Desai, A. R. & McConnell, S. K. Progressive restriction in fate potential by neural progenitors during cerebral cortical development. *Development* **127**, 2863–72 (2000).
26. Telley, L. *et al.* Sequential transcriptional waves direct the differentiation of newborn neurons in the mouse neocortex. *Science* **351**, 1443–1446 (2016).
27. Telley, L. *et al.* Temporal patterning of apical progenitors and their daughter neurons in the developing neocortex. *Science* **364**, (2019).
28. Moreau, M. X., Saillour, Y., Cwetsch, A. W., Pierani, A. & Causeret, F. Single-cell transcriptomics of the early developing mouse cerebral cortex disentangle the spatial and temporal components of neuronal fate acquisition. *Development* **148**, (2021).
29. Di Bella, D. J. *et al.* Molecular logic of cellular diversification in the mouse cerebral cortex. *Nature* **595**, 554–559 (2021).
30. Zimmer, C., Tiveron, M. C., Bodmer, R. & Cremer, H. Dynamics of Cux2 expression suggests that an early pool of SVZ precursors is fated to become upper cortical layer neurons. *Cerebral Cortex* **14**, 1408–1420 (2004).
31. Franco, S. J. *et al.* Fate-restricted neural progenitors in the mammalian cerebral cortex. *Science* **337**, 746–9 (2012).
32. Gil-Sanz, C. *et al.* Lineage Tracing Using Cux2-Cre and Cux2-CreERT2 Mice. *Neuron* **86**, 1091–1099 (2015).
33. García-Moreno, F. & Molnár, Z. Subset of early radial glial progenitors that contribute to the development of callosal neurons is absent from avian brain. *Proc Natl Acad Sci U S A* **112**, E5058-67 (2015).
34. Dominguez, M. H., Ayoub, A. E. & Rakic, P. POU-III transcription factors (Brn1, Brn2, and Oct6) influence neurogenesis, molecular identity, and migratory destination of upper-layer cells of the cerebral cortex. *Cerebral Cortex* **23**, 2632–2643 (2013).
35. Zahr, S. K. *et al.* A Translational Repression Complex in Developing Mammalian Neural Stem Cells that Regulates Neuronal Specification. *Neuron* **97**, 520-537.e6 (2018).
36. Zhu, X. *et al.* BRN2 as a key gene drives the early primate telencephalon development. *Sci Adv* **8**, 1–17 (2022).
37. Zheng, S. C. *et al.* Universal prediction of cell-cycle position using transfer learning. *Genome Biol* **23**, 1–27 (2022).
38. Bertrand, N., Castro, D. S. & Guillemot, F. Proneural genes and the specification of neural cell types. *Nat Rev Neurosci* **3**, 517–530 (2002).

39. Britz, O. *et al.* A role for proneural genes in the maturation of cortical progenitor cells. *Cerebral Cortex* **16**, (2006).
40. Chou, R. H., Yu, Y. L. & Hung, M. C. The roles of EZH2 in cell lineage commitment. *Am J Transl Res* **3**, 243–250 (2011).
41. Nieto, M. *et al.* Expression of Cux-1 and Cux-2 in the subventricular zone and upper layers II-IV of the cerebral cortex. *Journal of Comparative Neurology* **479**, 168–180 (2004).
42. Cubelos, B. *et al.* Cux-2 controls the proliferation of neuronal intermediate precursors of the cortical subventricular zone. *Cerebral Cortex* **18**, 1758–1770 (2008).
43. Shimojo, H., Ohtsuka, T. & Kageyama, R. Oscillations in Notch Signaling Regulate Maintenance of Neural Progenitors. *Neuron* **58**, 52–64 (2008).
44. Imayoshi, I. *et al.* Oscillatory control of factors determining multipotency and fate in mouse neural progenitors. *Science (1979)* **342**, 1203–1208 (2013).
45. Borrell, V. *et al.* Slit/Robo Signaling Modulates the Proliferation of Central Nervous System Progenitors. *Neuron* **76**, 338–352 (2012).
46. Castro, D. S. *et al.* Proneural bHLH and Brn Proteins Coregulate a Neurogenic Program through Cooperative Binding to a Conserved DNA Motif. *Dev Cell* **11**, 831–844 (2006).
47. Jayaraman, D., Bae, B. Il & Walsh, C. A. The genetics of primary microcephaly. *Annu Rev Genomics Hum Genet* **19**, 177–200 (2018).
48. Johnson, M. B. *et al.* Aspm knockout ferret reveals an evolutionary mechanism governing cerebral cortical size letter. *Nature* **556**, 370–375 (2018).
49. Saade, M., Morin, X., Onorati, M., Wilsch-Bräuninger, M. & Huttner, W. B. Primary Cilia and Centrosomes in Neocortex Development. *Front. Neurosci.* **15**, 755867 (2021).
50. Li, S., Hannenhalli, S. & Ovcharenko, I. De novo human brain enhancers created by single-nucleotide mutations. *Sci Adv* **9**, eadd2911 (2023).

Methods – additional references:

51. Levine, M. S. *et al.* Centrosome Amplification Is Sufficient to Promote Spontaneous Tumorigenesis in Mammals. *Dev Cell* **40**, 313-322.e5 (2017).
52. Moyer, T. C. & Holland, A. J. PLK4 promotes centriole duplication by phosphorylating STIL to link the procentriole cartwheel to the microtubule wall. *Elife* **8**, e46054 (2019).
53. Tang, X., Falls, D. L., Li, X., Lane, T. & Luskin, M. B. Antigen-retrieval procedure for bromodeoxyuridine immunolabeling with concurrent labeling of nuclear DNA and antigens damaged by HCl pretreatment. *Journal of Neuroscience* **27**, 5837–5844 (2007).
54. Wang, F. *et al.* RNAscope: A novel in situ RNA analysis platform for formalin-fixed, paraffin-embedded tissues. *Journal of Molecular Diagnostics* **14**, 22–29 (2012).
55. Long, J. Z., Lackan, C. S. & Hadjantonakis, A. K. Genetic and spectrally distinct in vivo imaging: Embryonic stem cells and mice with widespread expression of a monomeric red fluorescent protein. *BMC Biotechnol* **5**, 1–11 (2005).
56. Matsuda, T. & Cepko, C. L. Controlled expression of transgenes introduced by in vivo electroporation. *Proc Natl Acad Sci U S A* **104**, 1027–1032 (2007).
57. Schroeter, E. H., Kisslinger, J. A. & Kopan, R. Notch-1 signalling requires ligand-induced proteolytic release of intracellular domain. *Nature* **393**, 382–386 (1998).
58. Kim, D. S., Matsuda, T. & Cepko, C. L. A core paired-type and POU homeodomain-containing transcription factor program drives retinal bipolar cell gene expression. *Journal of Neuroscience* **28**, 7748–7764 (2008).

59. Saito, T. & Nakatsuji, N. Efficient gene transfer into the embryonic mouse brain using in vivo electroporation. *Dev Biol* **240**, 237–246 (2001).
60. Kawasaki, H., Iwai L., Tanno K., Rapid and efficient genetic manipulation of gyrencephalic carnivores using in utero electroporation. *Mol Brain.* **5**, 24 (2012).
61. Cao, J. *et al.* The single-cell transcriptional landscape of mammalian organogenesis. *Nature* **566**, 496–502 (2019).
62. Haghverdi, L., Lun, A. T. L., Morgan, M. D. & Marioni, J. C. Batch effects in single-cell RNA-sequencing data are corrected by matching mutual nearest neighbors. *Nat Biotechnol* **36**, 421–427 (2018).
63. Becht, E. *et al.* Dimensionality reduction for visualizing single-cell data using UMAP. *Nat Biotechnol* **37**, 38–47 (2019).
64. Molyneaux, B. J. *et al.* DeCoN: Genome-wide analysis of invivo transcriptional dynamics during pyramidal neuron fate selection in neocortex. *Neuron* **85**, 275–288 (2015).

Acknowledgments: We thank members of the Müller and Kolodkin laboratories for suggestions, reagents and technical help; Alex Kolodkin, Jakub Ziak and Cristina Gil-Sanz for critical comments on the manuscript; Caiying Guo for help in generating the *Brn1* floxed mice; Amanda Maxwell, Caroline Garrett and Eric Hutchinson for help with ferrets; Michele Pucak for imaging assistance; Linda Orzolek and Tyler J. Creamer for help with scRNAseq; Anna-Katerina Hadjantonakis, Connie Cepko and Raphael Kopan for plasmids; Ryoichiro Kageyama for the HES1 antibody; Andrew Holland for the γ-TUBULIN and Centrin antibodies. We are grateful to Michelle Monroe, Tajma Smith, Kaiping Zhang and Femi Cleola Villamor for assistance with mouse maintenance and genotyping. **Funding:** National Institutes of Health grant R01HG012357 and RF1MH121539 (UM)**. Author contributions:** Conceptualization: SB, UM; Methodology: SB, GSO'B, YX, LG, KN, RV, UM; Investigation: SB, GSO'B, YX, UM; Validation: SB, GSO'B, YX, UM; Visualization: SB; Formal analysis: SB, GSO'B, YX, UM; Data curation: SB, GSO'B, YX; Resources: KN, BB, RSS, CAW, UM; Supervision: UM; Project administration: UM; Funding acquisition: UM; Writing - original draft: SB, UM; Writing - review & editing: SB, YX, LG, KN, RV, BB, RSS, CAW, GSO'B, UM. **Competing interests:** The authors declare no competing or financial interests. **Data and materials availability:** All data are available in the main text or the supplementary information. Correspondence and requests for materials should be addressed to UM.

Figures:

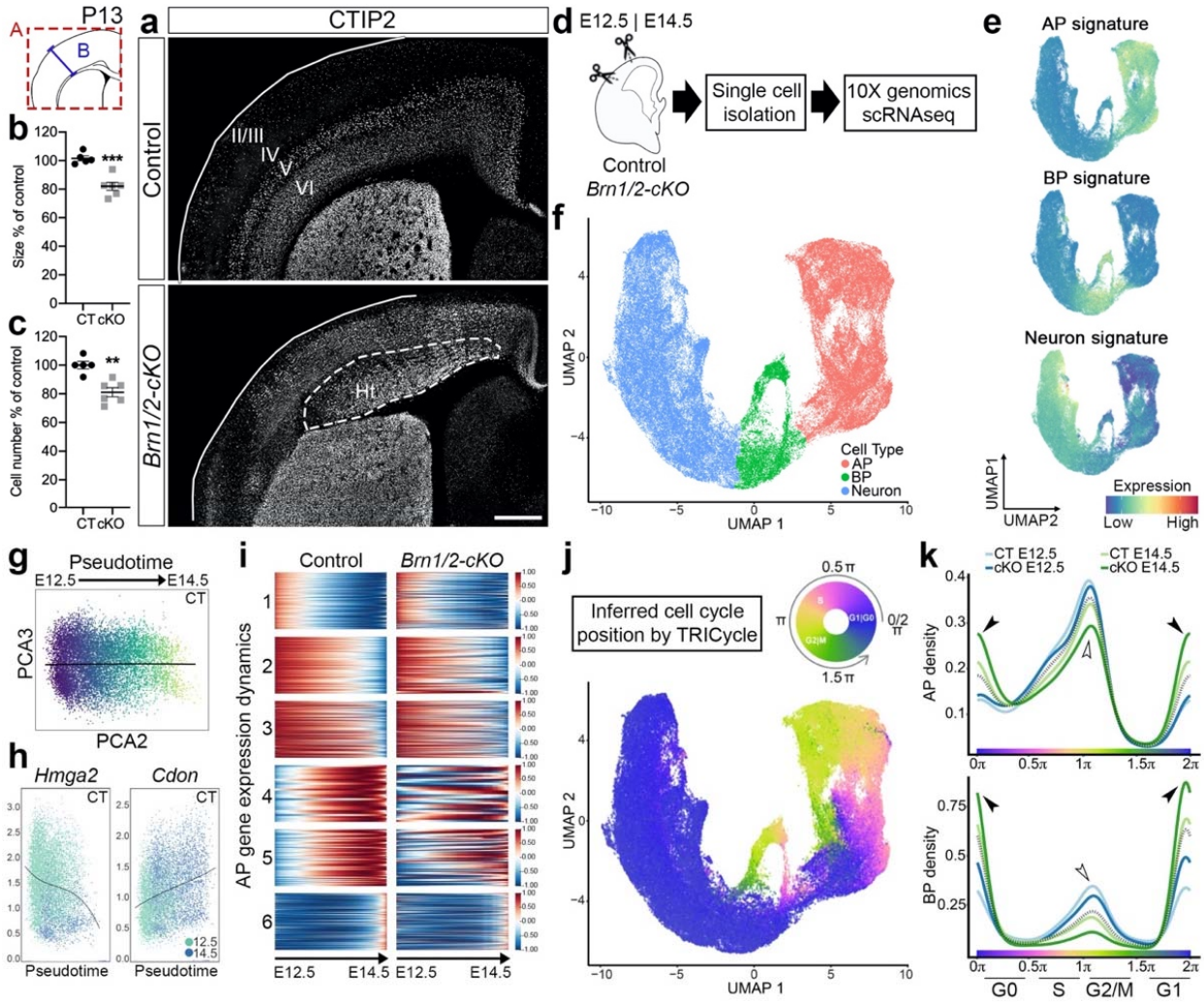

Fig. 1 BRN1/2 regulate cell cycle exit. a, Control and *Brn1/2-cKO* brains analyzed by CTIP2 immunolabeling at P13. Lines represent the limits of the cortical plate (CP); dashed lines outline cortical heterotopia (Ht). **b**, **c**, Cortical size (b) and total cell number (c) in control and *Brn1/2-cKO* cortices at P13 (n=5 CT, n=6 *cKO* mice; unpaired t-test). **d,** 10X genomics *scRNA-seq* in control and *Brn1/2-cKO* mice at E12.5 and E14.5. **e,** UMAP of gene signatures for AP, BP and neurons. **f,** UMAPs from control and *Brn1/2-cKO* cortices at E12.5 and E14.5 by cell type. **g,** Principal component analysis (PCA) of control AP transcriptional identity organization along the pseudotime axis. **h,** Expression of *Hmga2* and *Cdon* in control APs along the pseudotime axis. **i,** Cluster analysis of the gene expression dynamics for the APs along the pseudotime axis in control and *Brn1/2-cKO* mice (SI_1). **j,** UMAPs from control and *Brn1/2-cKO* cortices at E12.5 and E14.5 by TRIcycle analysis[37]. **k,** Cell cycle phase analysis from control and *Brn1/2-cKO* APs and BPs at E12.5 and E14.5 represented as cell density (Wilcoxon rank sum test: AP E12.5 p= 0.085; AP E14.5 p= 1.84e-15; BP E12.5 p=1.95e-06; BP E14.5 p<2.2e-16). Empty arrowheads point to reduced S-G2/M state in mutants, arrowheads to increased G1/G0 state. Values are mean ± SEM; **p<0.01, ***p<0.001; Scale bars: 500 µm.

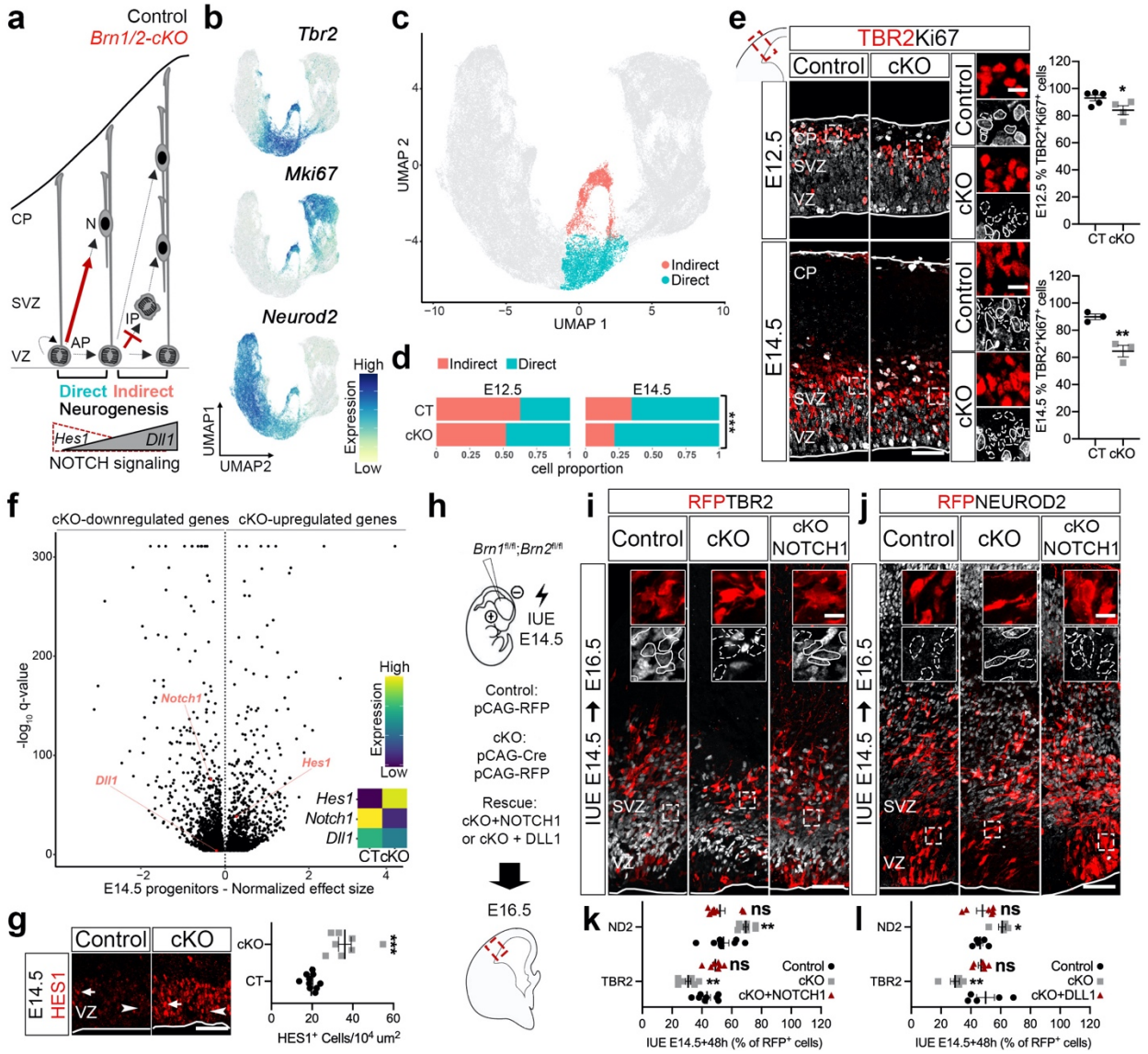

Fig. 2 BRN1/2 regulate the switch from direct to indirect neurogenesis via NOTCH signaling. a, Schematic of progenitor's neurogenic mode in control (black) and *Brn1/2-cKO* (red). **b,** UMAP of *Tbr2*, *MKi67 and Neurod2* expression in scRNAseq datasets. **c,** UMAP of cells going through indirect and direct neurogenesis in control and *Brn1/2-cKO* cortices at E12.5 and E14.5. **d,** Proportion of cells going through indirect and direct neurogenesis by age and genotype (Pearson's Chi-squared test – ***p<0.001). **e,** TBR2 (red) and Ki67 (grey) immunolabeling in control and *Brn1/2-cKO* cortical sections at E12.5 and E14.5 (E12.5: n=5 CT, n=4 *cKO* mice; E14.5: n=3 mice per group; unpaired t-test). Boxed area at higher magnification on the right. Lines and dashed lines circulating cells: expression or absence of Ki67, respectively. **f,** Volcano plot: differentially expressed genes between *Brn1/2-cKO* progenitors and controls at E14.5 highlighting NOTCH signaling-associated genes (Monocle3 VGAM test; SD=0.15; q<0.05; SI_5). **g,** HES1 (red) immunolabeling in the VZ of control and *Brn1/2-cKO* cortical sections at E14.5 (n=10 CT, n=8 *cKO* mice; unpaired t-test). **h,** IUE in *Brn1*$^{fl/fl}$;*Brn2*$^{fl/fl}$ mice at E14.5 with the indicated plasmids. **i, j,** Cell identities of the control, *Brn1/2-cKO* and *Brn1/2-cKO*+NOTCH1 condition analyzed by co-immunolabeling for RFP (red; to identify

electroporated cells) with TBR2 (i, grey) and NEUROD2 (j, grey) at E16.5. Boxed area: higher magnification in inserts. Lines and dashed lines outlining cells expressing or lacking expression of the indicated marker, respectively. **k**, **l,** RFP^+ cells expressing TBR2 and NEUROD2 at E16.5 in the control, *Brn1/2-cKO*, *Brn1/2-cKO*+NOTCH1 (k) and *Brn1/2-cKO*+DLL1 (l) condition (NOTCH1(k): n=8 CT, n=8 *cKO*, n=7 *cKO*+NOTCH1 mice; DLL1(l): n=5 CT, n=5 *cKO*, n=6 *cKO*+NOTCH1 mice; one-way ANOVA – Dunnett's multiple comparisons test; NOTCH1-TBR2: $F_{2,20}$=20.50; NOTCH1-NEUROD2: $F_{2,21}$=9.702; DLL1-TBR2: $F_{2,13}$=8.294; DLL1-NEUROD2: $F_{2,13}$=6.748). Low and top lines represent the limits of the VZ and CP, respectively. Values are mean ± SEM; ns, not significant; *p<0.05, **p<0.01, ***p<0.001. Scale bars: 50 µm (lower magnification), 10 µm (higher magnification).

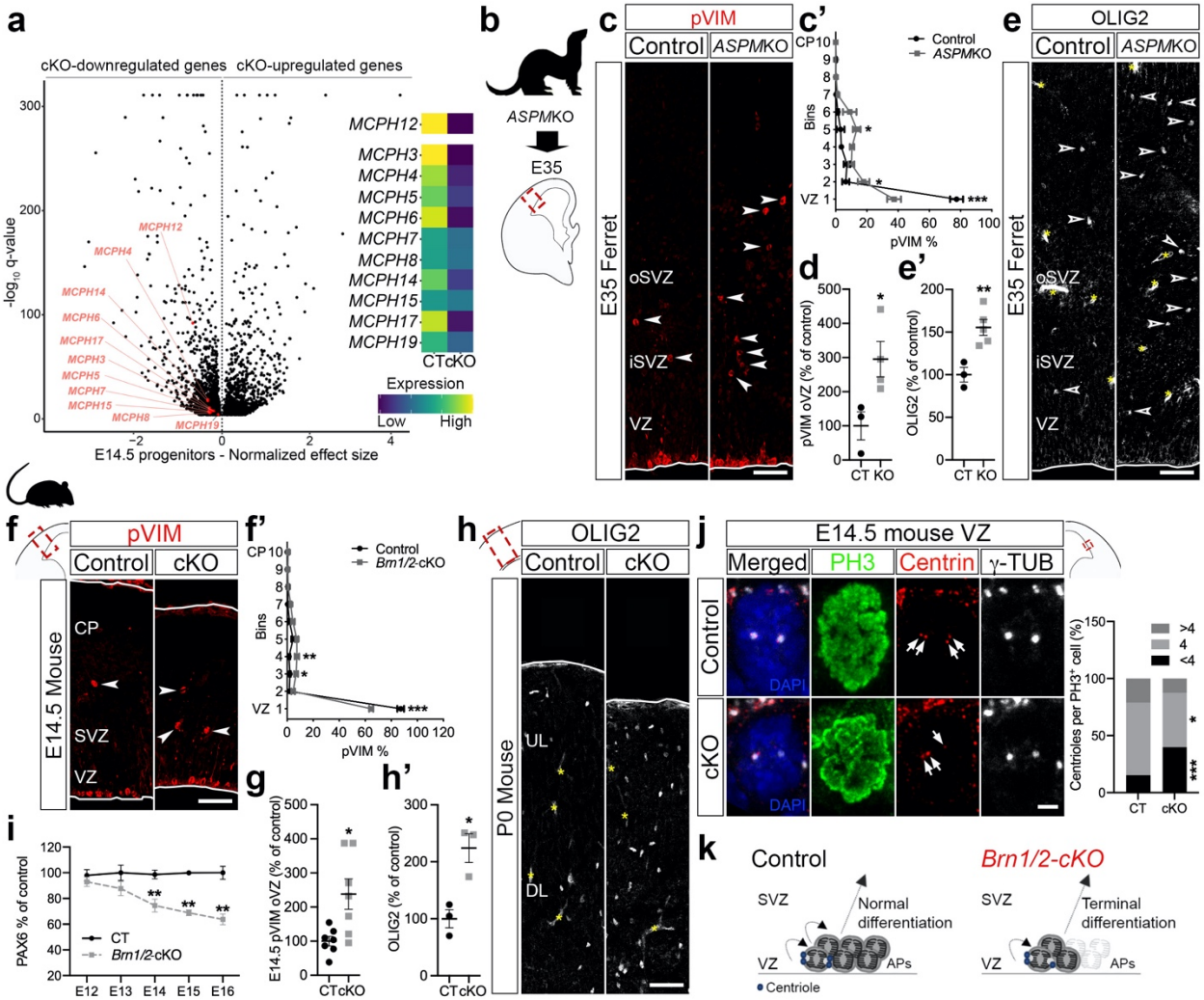

Fig. 3 BRN1/2 are required for the expression of microcephaly-associated genes and maintenance of the neuronal progenitor pool. a, Volcano plot: genes differentially expressed between *Brn1/2-cKO* and control progenitors at E14.5 highlighting primary microcephaly genes (Monocle3 VGAM test; SD=0.15; q<0.05; SI_5). **b,** Histological analysis at E35 in cortical sections of control and *ASPM*KO ferrets. **c,** pVIM immunolabeling in cortical sections of control and *ASPM*KO ferrets at E35. Arrowheads: pVIM$^+$ cells outside the VZ. **c',** Distribution of pVIM$^+$ cells in the cortex of control and *ASPM*KO ferrets (n=3 CT, n=4 KO ferrets; two-way ANOVA – Šídák's multiple comparisons test; $F_{9,50}$=19.02). **d,** pVIM$^+$ cells outside of the VZ (oVZ) in control and *ASPM*KO cortices (n=3 CT, n=4 KO ferrets; unpaired t-test). **e, e',** OLIG2 immunolabeling in cortical sections of control and *ASPM*KO ferrets at E35 (n=3 CT, n=5 KO ferrets; unpaired t-test). Empty arrowheads indicate OLIG2$^+$ cells. **f,** pVIM immunolabeling in cortical sections of control and *Brn1/2-cKO* mice at E14.5. Arrowheads: pVIM$^+$ cells outside the VZ. **f'**, Distribution of pVIM$^+$ cells in the cortex of control and *Brn1/2-cKO* mice (n=7 mice per group; two-way ANOVA – Šídák's multiple comparisons test; $F_{9,120}$=25.73). (**G**) pVIM$^+$ cells outside of the VZ (oVZ) in control and *Brn1/2-cKO* cortices (n=7 mice per group; unpaired t-test). **h, h',** OLIG2 immunolabeling in cortical sections of control and *Brn1/2-cKO* mice at P0 (n=3 mice per group; unpaired t-test). **i,** PAX6$^+$ cells in control and *Brn1/2-cKO* cortices from E12.5 to E16.5 (E12.5: n=6 CT and n=4 *cKO* mice; E13.5: n=5 CT and n=6 *cKO* mice; E14.5:

n=4 CT and n=5 *cKO* mice; E15.5: n=5 CT and n=3 *cKO* mice; E16.5: n=5 CT and n=3 *cKO* mice; unpaired t-test). **j,** Centriole number per $PH3^+$ cell in the VZ of control and *Brn1/2-cKO* mice at E14.5 (n=3 mice per group; unpaired t-test). Arrows indicate the centrioles. **k,** Schematic of centrosome function and progenitor cell differentiation in control (black) and *Brn1/2-cKO* (red). Low and top lines represent the limits of the VZ and CP, respectively. Yellow asterisks indicate auto-fluorescent blood vessels. Values are mean ± SEM; $*p<0.05$, $**p<0.01$, $***p<0.001$. Scale bars: 50 µm (C, E, F and H), 2 µm (J).

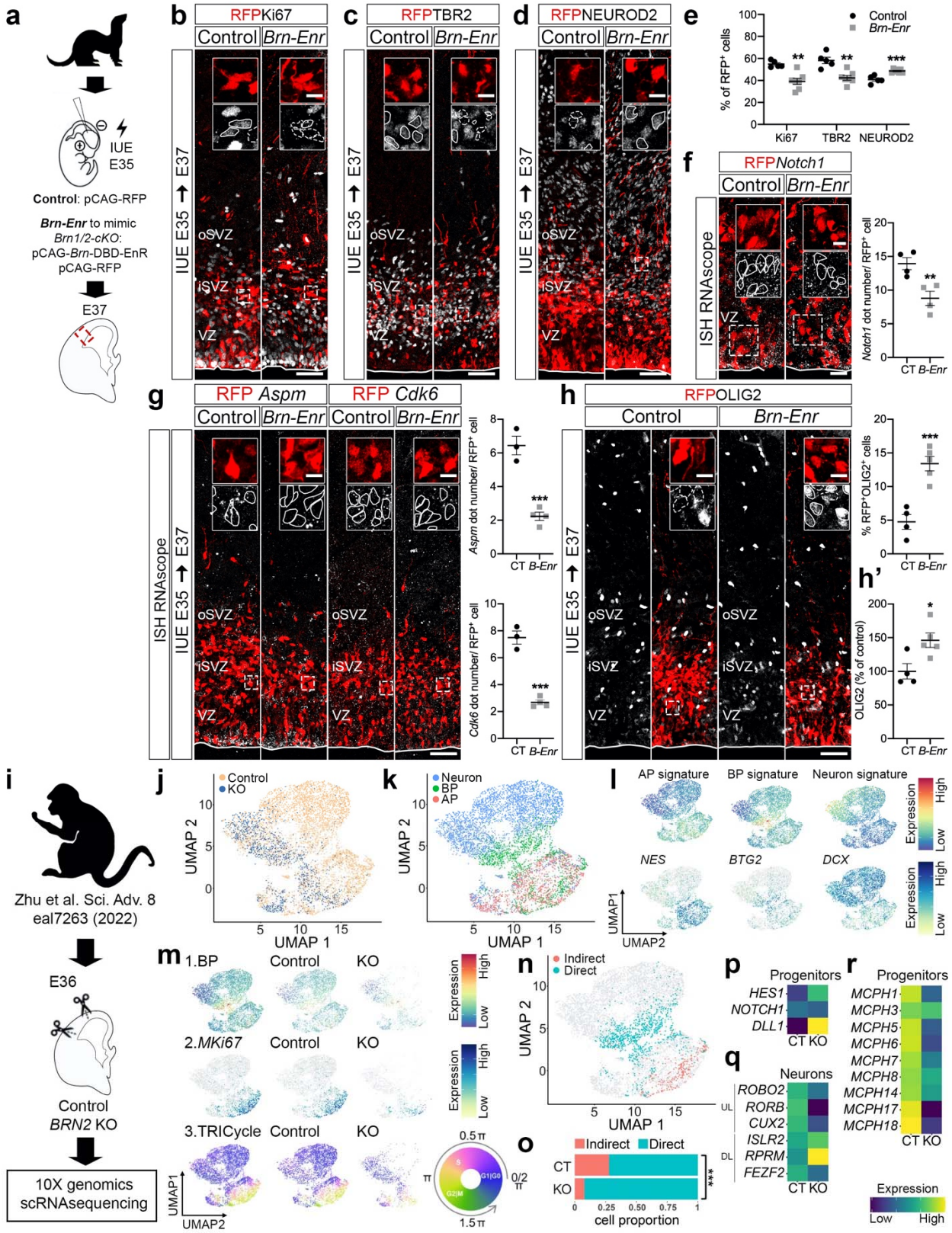

Fig. 4 BRN1/2 function is conserved across mammalian species. a, IUE in wild-type ferrets at E35 with the indicated plasmids. **b-d**, Cell identities in the control and *Brn-Enr* condition analyzed by co-immunolabeling of RFP (red) with Ki67 (b, grey), TBR2 (c, grey) and

NEUROD2 (d, grey) at E37. Boxed area: higher magnification in inserts. Lines and dashed lines outline cells expressing or not expressing the indicated marker, respectively. **e,** RFP^+ cells expressing Ki67, TBR2 and NEUROD2 in the electroporated somatosensory cortex (n=4 CT, n=7 *Brn-Enr* ferrets; unpaired t-test). **f,** *Notch1* (grey*)* expression by RNAscope and RFP (red) expression by immunolabeling in the VZ of the electroporated somatosensory cortex. Boxed area: higher magnification in inserts. Lines outline RFP^+ cells quantified for *Notch1* mRNA expression (n=4 ferrets per group; unpaired t-test). **g,** *Aspm* or *Cdk6* (grey*)* expression by RNAscope and RFP (red) expression by immunolabeling in the electroporated somatosensory cortex. Boxed area: higher magnification in inserts. Lines outline RFP^+ cells quantified for *Aspm* or *Cdk6* mRNA expression (n=3 CT, n=4 *Brn-Enr* ferrets; unpaired t-test). **h,** RFP^+ cells expressing OLIG2 (gray) in the electroporated somatosensory cortex (n=4 CT, n=5 *Brn-Enr* ferrets; unpaired t-test). Boxed area: higher magnification in inserts. Lines and dashed lines circulating cells: expression or absence of OLIG2, respectively. **h',** Total $OLIG2^+$ cells in the electroporated somatosensory cortex (n=4 CT, n=5 *Brn-Enr* ferrets; unpaired t-test). **i,** ScRNAseq DATA from E36 cortex of control and *BRN2*KO cynomolgus monkey[36] re-analyzed using the same pipeline we used for the analysis in mice. **j**, **k,** UMAP of scRNAseq from control and *BRN2*KO cortices by genotype (j) and cell type (k). **l,** UMAP of gene signatures for AP (e.g., *NES*), BP (e.g., *BTG2*) and neurons (e.g., *DCX*) in control and *BRN2*KO cortices. **m,** UMAP of BP signature (1), *MKi67* expression (2) and TRIcycle score (3) in control and *BRN2*KO cortices. **n,** UMAP of cells going through indirect and direct neurogenesis in control and *BRN2*KO cortices. **o,** Proportion of cells going through indirect and direct neurogenesis by genotype (Pearson's Chi-squared test – ***$p<0.001$). **p,** Expression of NOTCH signaling-associated genes in control and *BRN2*KO progenitors. **q,** Expression of the indicated cortical UL and DL neuronal marker genes in control and *BRN2*KO neurons. **r,** Expression of primary microcephaly genes differentially affected in *BRN2*KO progenitors compared to controls. Values are mean ± SEM; *$p<0.05$, **$p<0.01$, ***$p<0.001$. Scale bars: 50 µm (lower magnification), 10 µm (higher magnification).

Extended Data:

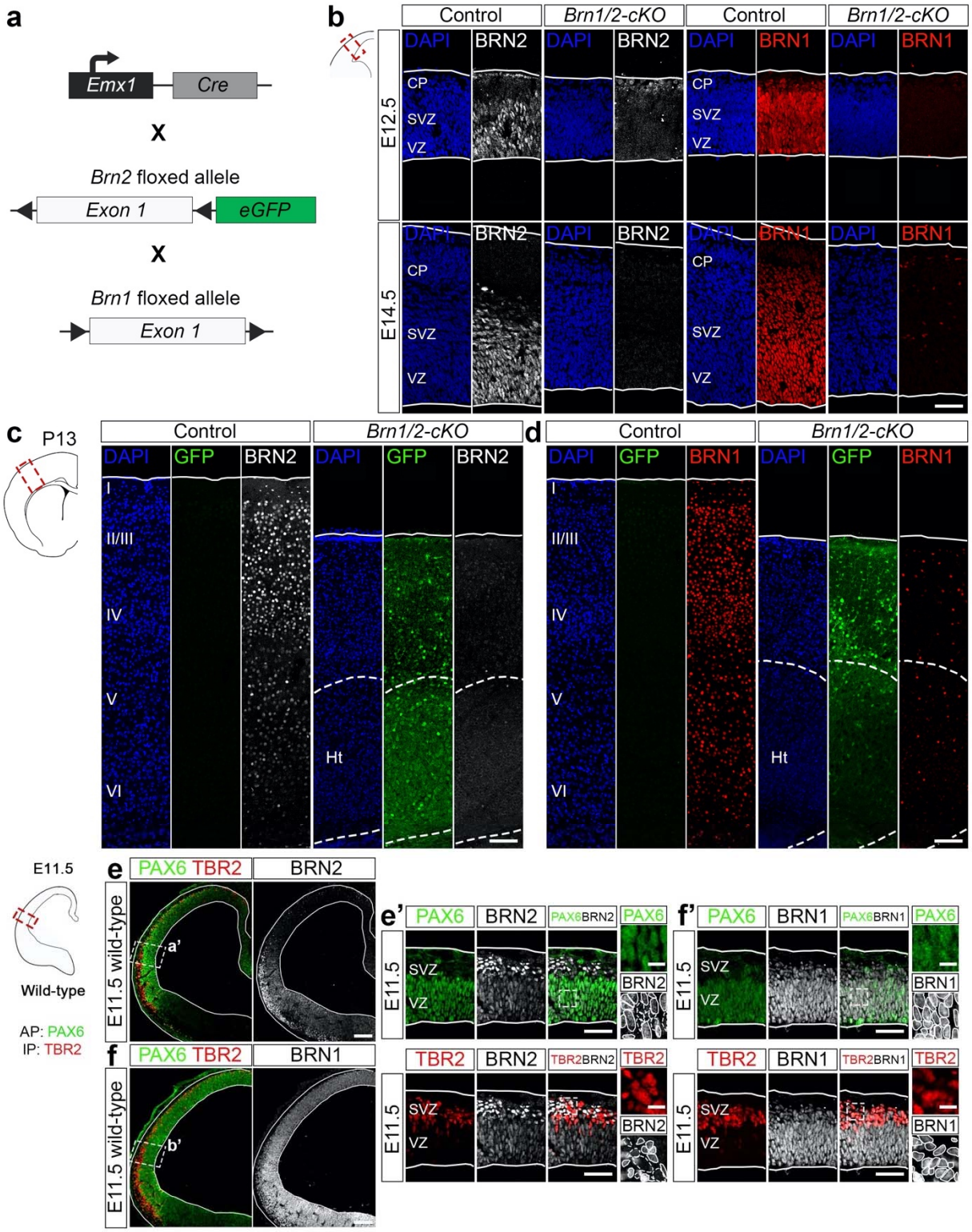

Extended Data Fig. 1 BRN1 and BRN2 expression. **a,** Diagram of experimental strategy. *Emx1-Cre* mice were crossed with *Brn1*$^{fl/fl}$;*Brn2*$^{fl/fl}$ mice to inactivate *Brn1* and *Brn2* in the dorsal telencephalon. **b,** DAPI staining (blue) and BRN2 (grey) and BRN1 (red) immunolabeling in

cortical sections of control and *Brn1/2-cKO* mice at E12.5 and E14.5. Low and top lines represent the limits of the VZ and CP, respectively. Scale bar: 50 µm. **c, d,** DAPI staining (blue) and GFP (green), BRN2 (c, grey) and BRN1 (d, red) immunolabeling in cortical sections of control and *Brn1/2-cKO* mice at P13. BRN1 is also expressed in interneurons and therefore those cells, that are not recombined in *Emx1-Cre* mice, remain positive for BRN1 in the cortex of *Brn1/2-cKO* mice at P13 (d). Neocortical cell layers I-VI are indicated. Lines represent the limits of the cortical plate; Dashed lines outline the cortical heterotopia (Ht). Scale bar: 100 µm. **e, f,** Overview of E11.5 wild-type brains labeled for DAPI (blue), PAX6 (green), TBR2 (red), BRN2 (e, grey) and BRN1 (f, grey). Meningeal and ventricular border indicated by white lines. Scale bar: 100 µm. **e', f',** Higher magnification view for TBR2 (red), PAX6 (green), BRN2 (e', grey) or BRN1 (f', grey) immunolabeling in the squared area highlighted in e or f, respectively. Boxed area shown at higher magnification on the rightmost panels. $TBR2^+$ and $PAX6^+$ cells expressing or lacking BRN1/2 expression are outlined by lines or dashed lines, respectively. Scale bars: 50 µm (lower magnification), 10 µm (higher magnification).

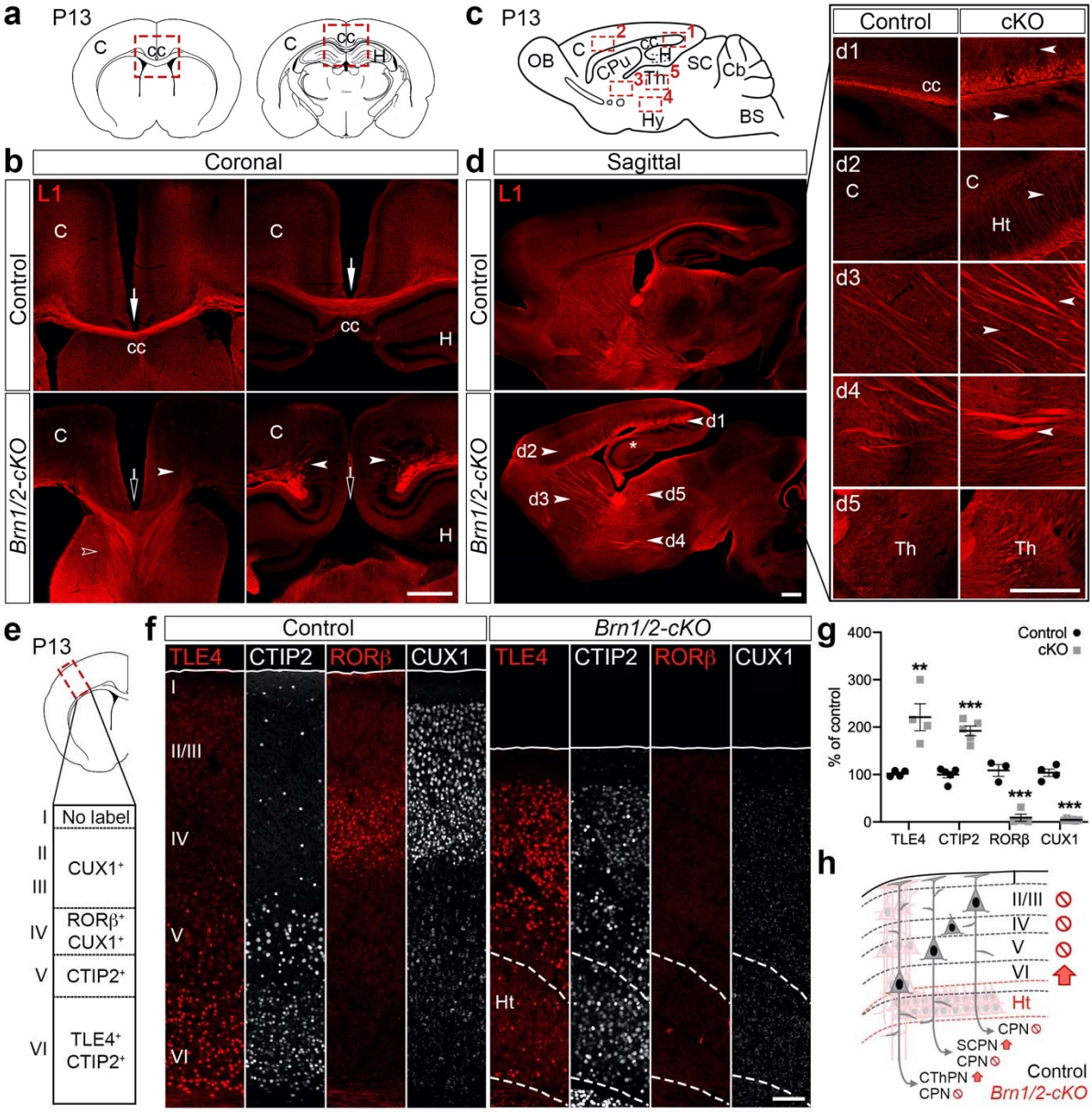

Extended Data Fig. 2 BRN1/2 are essential for proper neuronal specification and circuit development in the neocortex. a, Schematic of coronal brain sections at two histological levels highlighting the corpus callosum (cc). C, cortex; H, hippocampus. **b,** Cc of control and *Brn1/2-cKO* mice at different histological levels (500µm intervals) analyzed by L1 immunolabeling (red) at P13. Open arrows indicate absent cc and ventral misrouting of $L1^+$ projections in *Brn1/2-cKO* mice. Arrowheads indicate misrouting and abnormal defasciculation of $L1^+$ neurons in *Brn1/2-cKO* mice. **c,** Schematic of a midsagittal brain section highlighting the cc (1), cortex (C, 2), subcortical projections (3), hypothalamus (Hy, 4) and thalamus (Th, 5). OB, olfactory bulb; SC, superior colliculus; Cb, cerebellum; BS, brain stem. **d,** Neuronal projections of control and *Brn1/2-cKO* mice in midsagittal brain sections analyzed by L1 immunolabeling at P13. Arrowheads point to morphological changes in the *Brn1/2-cKO* brains. Numbers indicate areas shown in panel d1-d5. d1, absent cc; d2, cortical neuronal heterotopia (Ht); d3, more $L1^+$ neuronal fibers projecting to subcortical areas; d4, more disorganized $L1^+$ neuronal fibers

projecting to subcortical areas; d5, more $L1^+$ neuronal fibers targeting the thalamus; *disorganized hippocampus as previously described[18]. **e,** Schematic of a coronal brain section highlighting the somatosensory cortex analyzed at P13 by immunolabeling of the indicated molecular markers. **f, g,** Cortical layers of control and *Brn1/2-cKO* mice analyzed by TLE4 (layer VI, red), CTIP2 (layer VI, V and interneurons, grey), RORβ (layer IV, red) and CUX1 (layer IV and II/III, grey) immunolabeling (TLE4: n=4 mice per group, CTIP2: n=5 mice per group, RORβ: n=3 CT, n=4 *cKO* mice, CUX1: n=4 CT, n=6 *cKO* mice; values are mean ± SEM; unpaired t-test; $**p<0.01$, $***p<0.001$). Neocortical cell layers I-VI are indicated. Lines represent the limits of the cortical plate (CP); dashed lines represent the limits of the cortical heterotopia (Ht). **h,** Schematic of cortical projection neurons in *Brn1/2-cKO* mice (red) and controls (black). Scale bars: 500 µm (b, d, d1-d5), 100 µm (f).

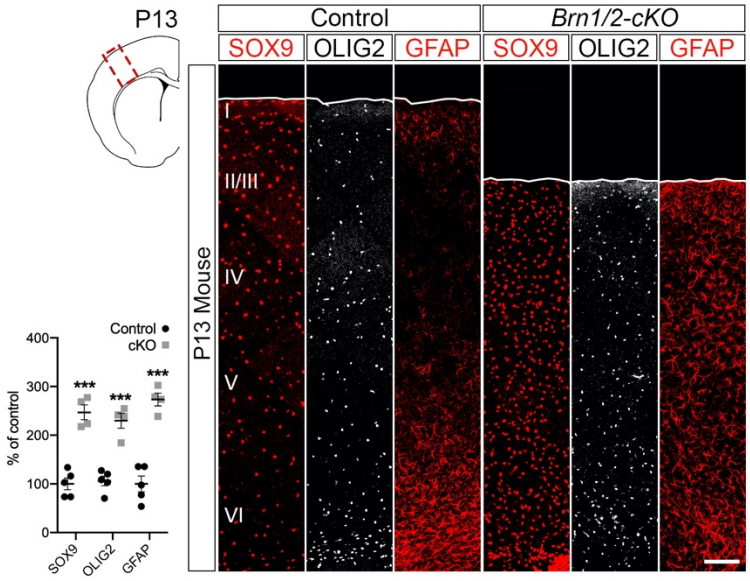

Extended Data Fig. 3 Glial cells are increased in *Brn1/2-cKO*. Schematic of a coronal brain section highlighting the somatosensory cortex analyzed at P13 by immunolabeling of the indicated molecular markers. SOX9 (red), OLIG2 (grey) and GFAP (red) immunolabeling in cortical sections of control and *Brn1/2-cKO* mice. Neocortical cell layers I-VI are indicated. Lines represent the limits of the cortical plate (n=5 CT, n= 4 *cKO*mice; values are mean ± SEM; unpaired t-test; ***p<0.001). Scale bars: 100 µm.

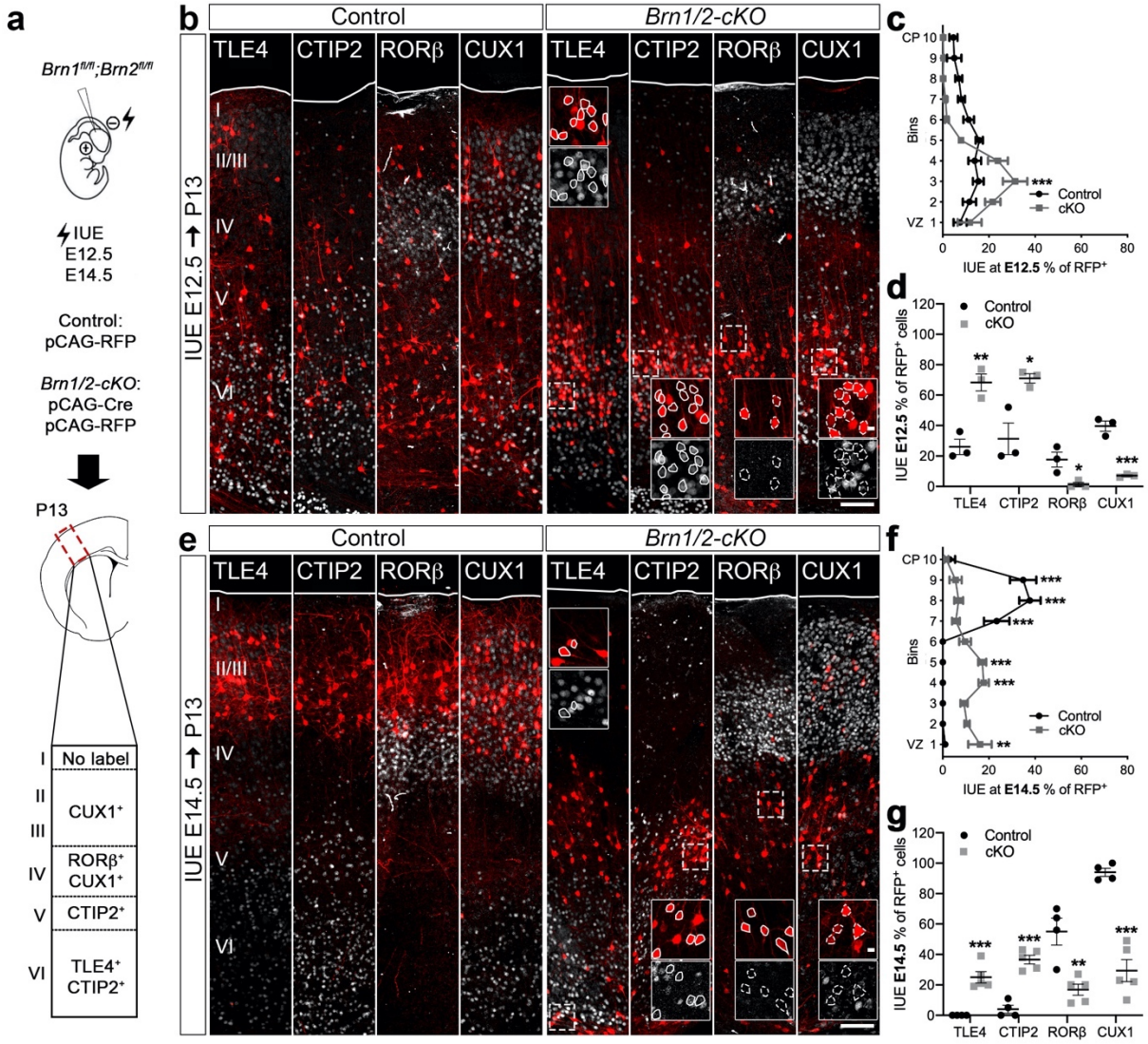

Extended Data Fig. 4 BRN1/2 regulate the competence of progenitor cells to generate ULNs. a, IUE in *Brn1*$^{fl/fl}$;*Brn2*$^{fl/fl}$ mice at E12.5 and E14.5 with the indicated plasmids. **b, e,** Neuronal identities of control and *Brn1/2-cKO* condition analyzed by co-immunolabeling of RFP (red) to identify electroporated cells with TLE4, CTIP2, RORβ and CUX1 (grey) at P13 after IUE at E12.5 (b) or E14.5 (e). Lines represent the limits of the CP. Boxed area: higher magnification in inserts. Lines outline cells expressing DLN markers; dashed lines outline cells not expressing ULN markers. **c, f,** Distribution of RFP$^+$ neurons in the somatosensory cortex at P13 after IUE at E12.5 (c) and E14.5 (f) (E12.5: n=3 mice per group; E14.5: n=4 CT, n=5 *cKO* mice; two-way ANOVA – Šídák's multiple comparisons test; E12.5: $F_{9,60}$=5.980; E14.5: $F_{9,70}$=24.90). **d, g,** RFP$^+$ neurons expressing the indicated marker genes at P13 after IUE at E12.5 (d) and E14.5 (g) (E12.5: n=3 mice per group, E14.5: n=4 CT, n=5 *cKO* mice; unpaired t-test). Values are mean ± SEM; **p*<0.05, ***p*<0.01, ***p<0.001. Scale bars: 100 µm (lower magnification), 10 µm (higher magnification).

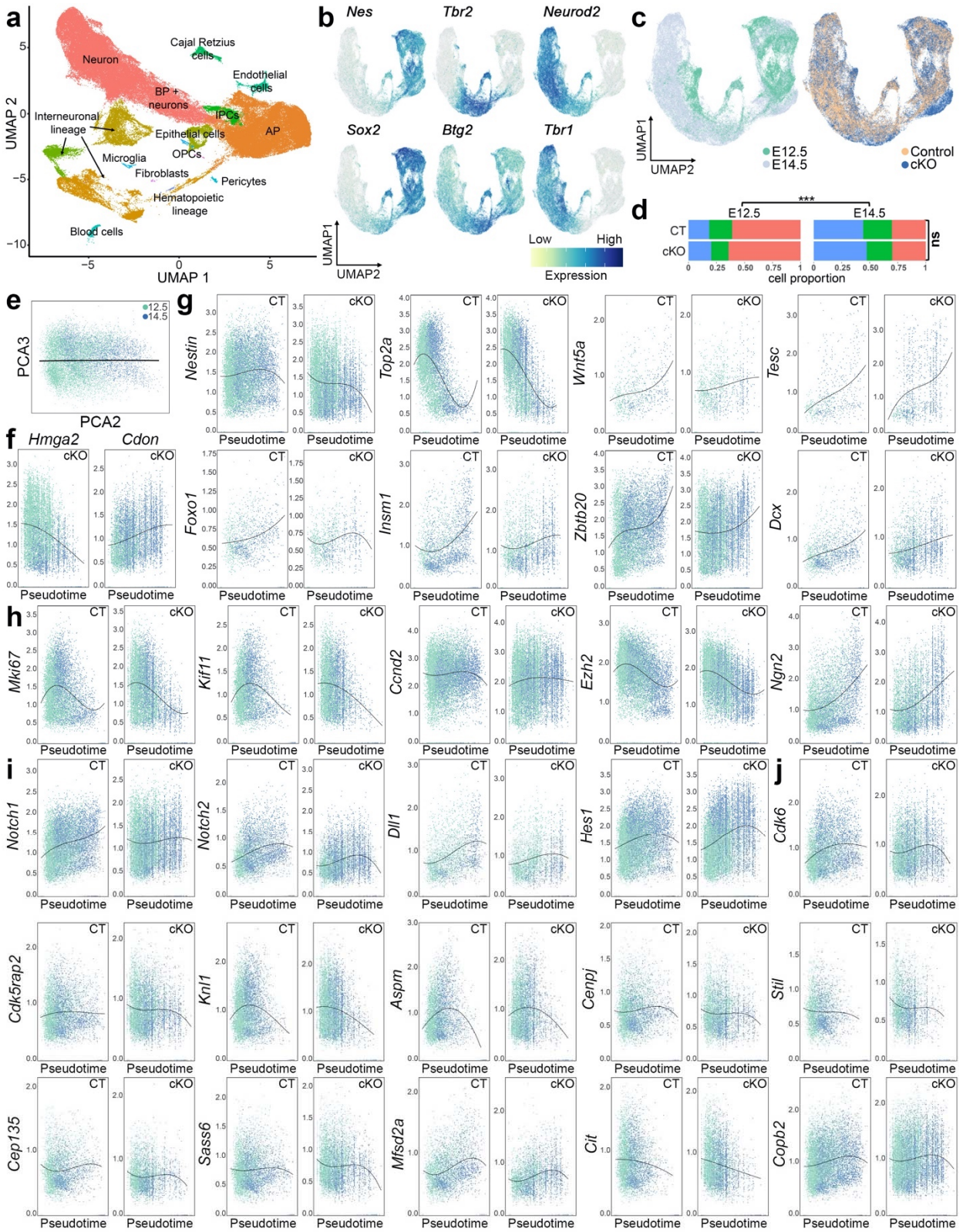

Extended Data Fig. 5 Altered transcriptional programs in cortical progenitors of *Brn1/2-cKO* mice a, UMAP of scRNAseq data of all cortical cells sequenced at E12.5 and E14.5. BP, basal progenitors; IPCs, intermediate progenitor cells; AP, apical progenitors; OPCs,

oligodendrocyte precursor cells. **b,** UMAP of gene signatures for AP (e.g., *Nes*, *Sox2*), BP (e.g., *Tbr2*, *Btg2*) and neurons (e.g., *Neurod2*, *Tbr1*). (**c,**) UMAP of scRNAseq data from control and *Brn1/2-cKO* cortices at E12.5 and E14.5, by age and genotype. **d,** Proportion of cell types by age and genotype (total cell numbers between genotypes compared by unpaired t-test – ns, not significant; cell proportions between ages and different genotypes compared by Pearson's Chi-squared test – ***$p<0.01$). **e,** PCA of control AP age identity organization along the pseudotime axis. **f,** Expression of *Hmga2* and *Cdon* in *Brn1/2-cKO* APs along the pseudotime axis. **g,** Examples of different gene expression dynamics in control and *Brn1/2-cKO* APs along the pseudotime axis. **h, i, j,** Expression of cell cycle-associated genes (h), NOTCH signaling-associated genes (i) and microcephaly-associated genes (j) in *Brn1/2-cKO* APs along the pseudotime axis.

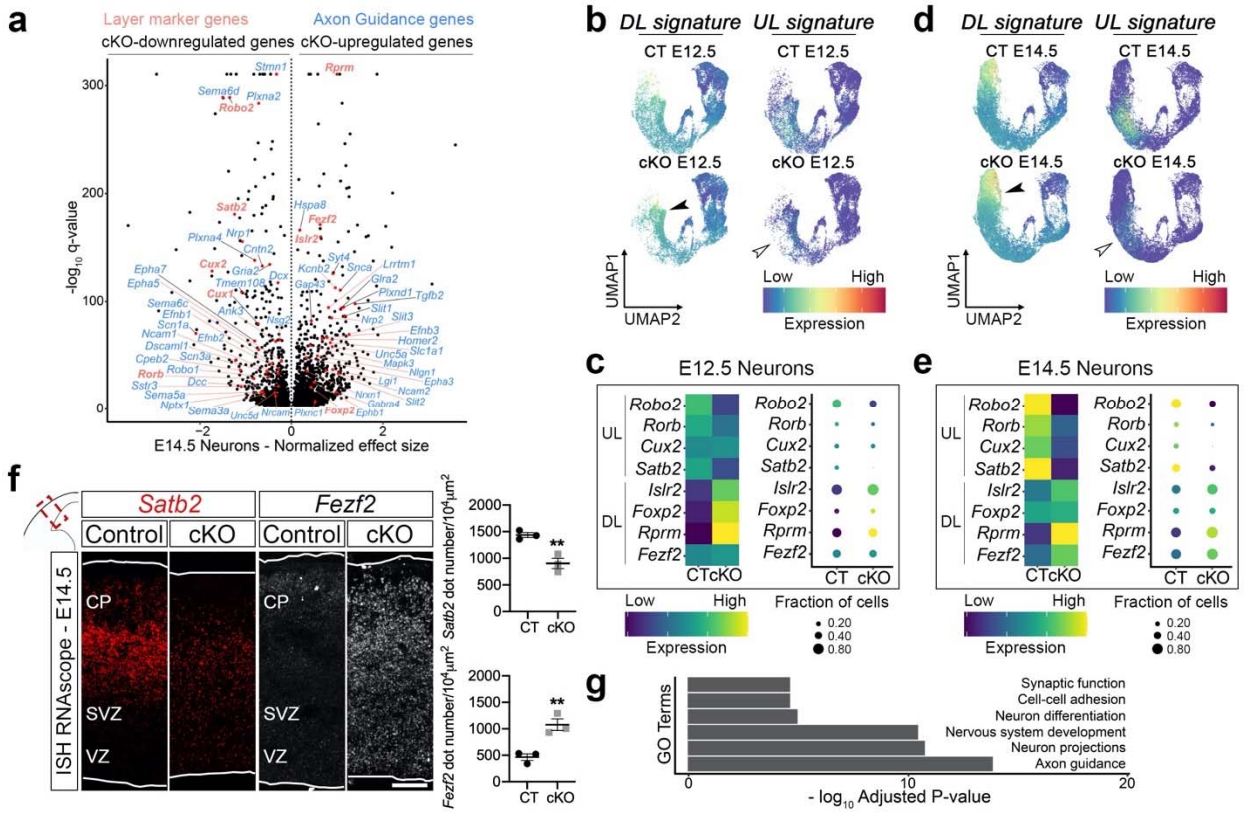

Extended Data Fig. 6 Changes in the transcriptional programs of the *Brn1/2-cKO* cortical progenitors favors the production of DLNs at E12.5 and E14.5. a, Volcano plot: genes differentially expressed between *Brn1/2-cKO* and control neurons at E14.5 highlighted for layer marker and axon guidance genes (Monocle3 VGAM test; SD=0.15; q<0.001; SI_2). **b, d,** UMAP of DL and UL gene signature in the scRNAseq datasets from control and *Brn1/2-cKO* cortices at E12.5 (b) and E14.5 (d). Empty arrowheads point to reduced expression of UL gene signature in mutants, arrowheads to increased expression of DL gene signature. **c, e,** Expression of the indicated cortical UL and DL marker genes in control and *Brn1/2-cKO* neurons at E12.5 (c) and E14.5 (e). **f,** RNAscope for *Fezf2* and *Satb2* in control and *Brn1/2-cKO* cortical sections at E14.5 (n=3 mice per group; values are mean ± SEM; unpaired t-test; **p<0.01). **g,** Some of the most relevant gene ontology (GO) terms differentially affected in *Brn1/2-cKO* neurons compared to controls at E14.5. Low and top lines represent the limits of the VZ and CP, respectively. Scale bar: 50 µm.

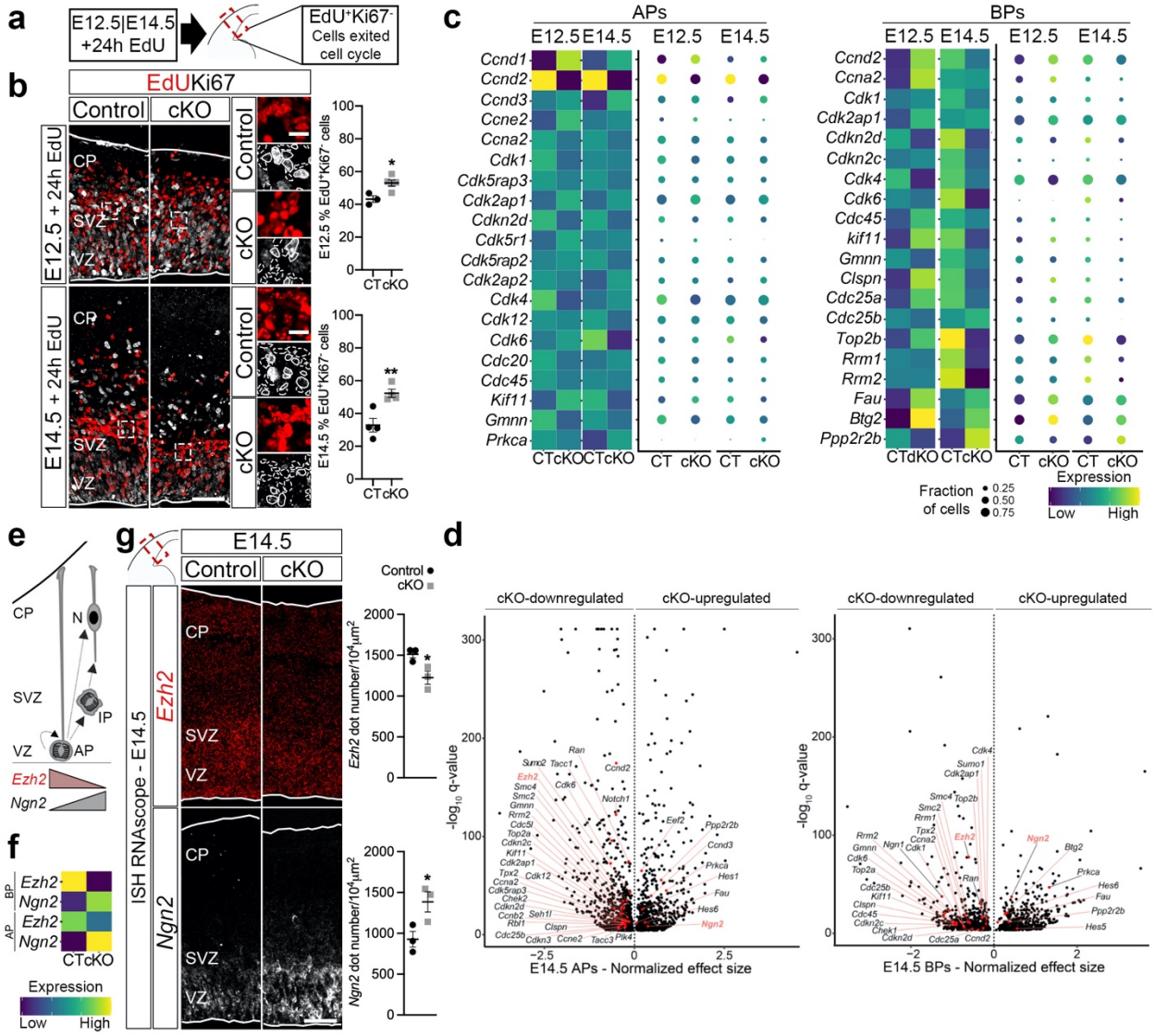

Extended Data Fig. 7 Reduction in proliferation rate and precocious cell cycle exit of cortical progenitors in *Brn1/2-cKO* mice. a, Schematic of the experimental strategy. E12.5 and E14.5 brains were analyzed by EdU and Ki67 immunolabeling 24h after intraperitoneal injection of EdU. **b,** EdU (red) and Ki67 (grey) immunolabeling in control and *Brn1/2-cKO* cortical sections at E12.5 and E14.5 (E12.5: n=3 CT, n=5 *cKO* mice; E14.5: n=4 mice per group; unpaired t-test). Boxed area at higher magnification on the right. Lines and dashed lines circulating the cells show expression or absence of Ki67, respectively. **c,** Expression of cell cycle-associated genes in *Brn1/2-cKO* APs and BPs compared to control at E12.5 and E14.5. **d,** Volcano plots: genes differentially expressed between *Brn1/2-cKO* and control APs and BPs at E14.5 highlighted for cell cycle-associated genes (Monocle3 VGAM test; SD=0.15; q<0.001; SI_3 and SI_4). **e,** Schematic of progenitors dividing and differentiating into neurons. **f,** Expression of *Ezh2* and *Ngn2* at E14.5 in control and *Brn1/2-cKO* APs and BPs as determined by scRNAseq. **g,** RNAscope for *Ezh2* (red) and *Ngn2* (grey) in control and *Brn1/2-cKO* cortical sections at E14.5 (n=3 mice per group; unpaired t-test). Low and top lines represent the limits of

the VZ and CP, respectively. Values are mean ± SEM; *$p<0.05$, **$p<0.01$, ***$p<0.001$; Scale bars: 50 µm (lower magnification), 10 µm (higher magnification).

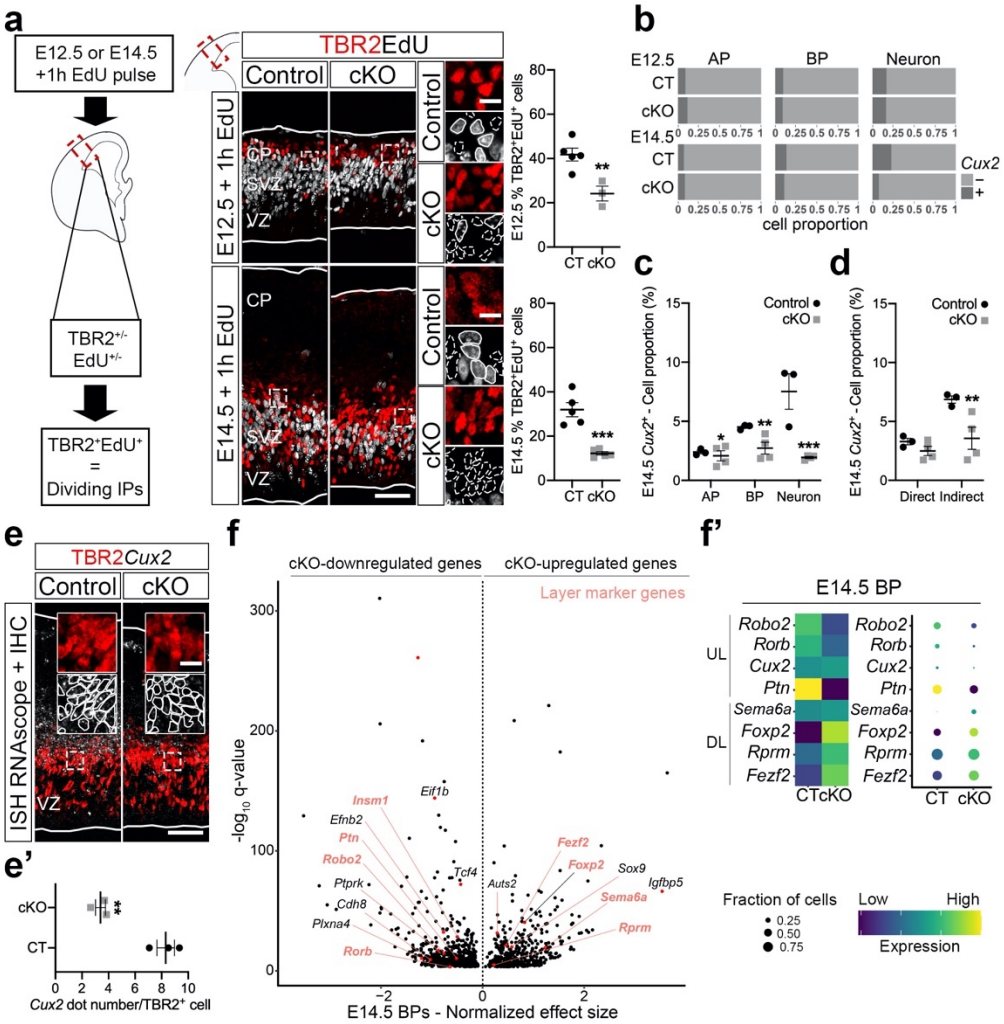

Extended Data Fig. 8 BRN1/2 regulate the balance between direct and indirect neurogenesis affecting the generation of a specific type of BPs. a, TBR2 (red) and EdU (grey) immunolabeling in control and *Brn1/2-cKO* cortical sections at E12.5 and E14.5 (E12.5: n=5 CT, n=3 *cKO* mice; E14.5: n=5 mice per group; unpaired t-test). Boxed area at higher magnification on the right. Lines and dashed lines circulating cells: expression or absence of EdU, respectively. **b,** Proportion of AP, BP and neurons expressing *Cux2* in control and *Brn1/2-cKO* cortices at E12.5 and E14.5. **c,** Proportion of AP, BP and neurons expressing *Cux2* in control and *Brn1/2-cKO* cortices at E14.5 (n ≥ 3 mice per group; Pearson's Chi-squared test). **d,** Proportion of cells undergoing direct and indirect neurogenesis expressing *Cux2* in control and *Brn1/2-cKO* cortices at E14.5 (n ≥ 3 mice per group; Pearson's Chi-squared test). **e, e',** *Cux2* (grey) expression by RNAscope and TBR2 (red) expression by immunolabeling in control and *Brn1/2-cKO* cortical sections at E14.5 (n=3 mice per group; unpaired t-test). Boxed area: higher magnification in inserts. Lines oultline TBR2$^+$ cells quantified for *Cux2* mRNA expression. **f,** Volcano plot: genes differentially expressed between *Brn1/2-cKO* and control BPs at E14.5 highlighted for layer marker genes (Monocle3 VGAM test; SD=0.15; q<0.001; SI_4). **f',** Expression of the indicated cortical UL and DL marker genes in control and *Brn1/2-cKO* BPs compared to controls at E14.5. Low and top lines represent the limits of the VZ and CP, respectively. Values are mean ± SEM;

*p<0.05, **p<0.01, ***p<0.001. Scale bars: 50 µm (lower magnification), 10 µm (higher magnification).

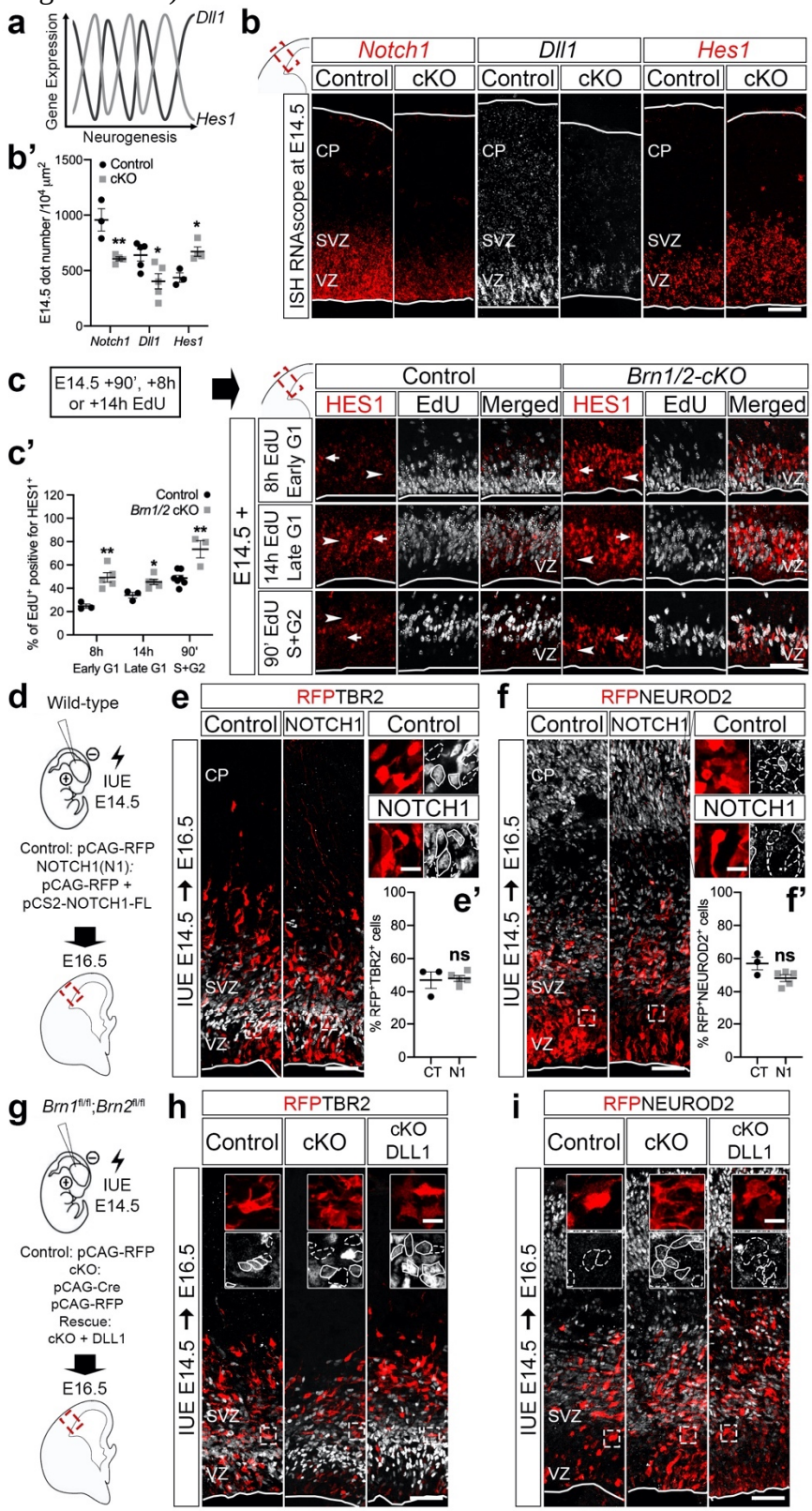

Extended Data Fig. 9 BRN1/2 are essential to maintain NOTCH signaling balanced during

neurodevelopment. a, Expression of HES1 and DLL1 in neural progenitors is oscillatory, which is critical for the maintenance of neural progenitors[43,44]. **b, b',** RNAscope for *Notch1* (red), *Dll1* (grey) and *Hes1* (red) in control and *Brn1/2-cKO* cortical sections at E14.5 (*Notch1* and *Hes1*: n=3 CT, n=4 *cKO* mice; *Dll1*: n=5 mice per group; unpaired t-test). **c,** E14.5 brains were collected 90', 8h or 14h after intraperitoneal injection of EdU. HES1 (red) and EdU (grey) immunolabeling in control and *Brn1/2-cKO* cortical sections at early G1 (8h EdU), late G1 (14h EdU) and S+G2 (90' EdU). Cells expressing HES1 at high and low levels are indicated by arrows and arrowheads, respectively. **c',** $HES1^+/EdU^+$ cells in control and *Brn1/2-cKO* cortices at early G1 (8h EdU), late G1 (14h EdU) and S+G2 (90' EdU) (8h and 14h: n=3 CT, n=5 *cKO* mice; 90': n=7 CT, n=3 *cKO* mice; unpaired t-test). **d,** IUE in wild-type mice at E14.5 with the indicated plasmids. **e, f,** Cell identities of the control and NOTCH1 condition analyzed by co-immunolabeling of RFP (red) with TBR2 (e, grey) and NEUROD2 (f, grey) at E16.5. Boxed area at higher magnification on the right. **e', f',** RFP^+ cells expressing TBR2 (e') and NEUROD2 (f') (n=3 CT, n=5 N1 mice; unpaired t-test). **g,** IUE in $Brn1^{fl/fl}$;$Brn2^{fl/fl}$ mice at E14.5 with the indicated plasmids. **h, i,** Cell identities of the control, *Brn1/2-cKO* and *Brn1/2-cKO*+DLL1 condition analyzed by co-immunolabeling of RFP (red) with TBR2 (h, grey) and NEUROD2 (i, grey) at E16.5. Boxed area: higher magnification in inserts. Lines and dashed lines outlining cells expressing or lacking expression of the indicated marker, respectively. Low and top lines represent the limits of the VZ and CP, respectively. Values are mean ± SEM; ns, not significant; $*p<0.05$, $**p<0.01$. Scale bars: 50 µm (lower magnification), 10 µm (higher magnification).

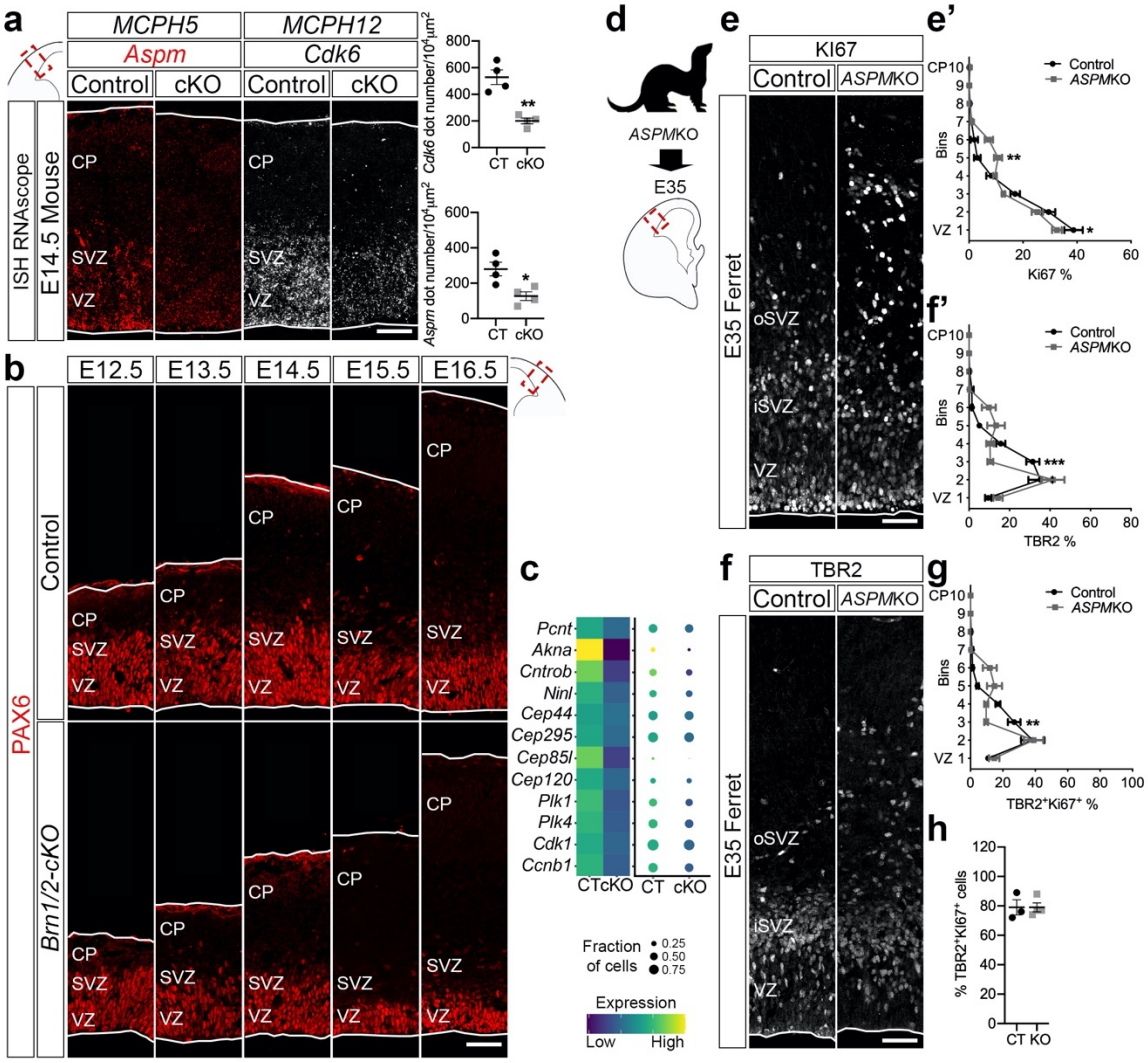

Extended Data Fig. 10 BRN1/2 are required for the expression of microcephaly-associated genes and maintenance of the neuronal progenitor pool. a, RNAscope for *Aspm* (red) and *Cdk6* (grey) in control and *Brn1/2-cKO* cortical sections at E14.5 (n=4 mice per group; unpaired t-test). **b,** PAX6 immunolabeling in control and *Brn1/2-cKO* cortical sections from E12.5 to E16.5. **c,** Expression of centrosome-associated genes in *Brn1/2-cKO* compared to control progenitors at E14.5. **d,** Histological analysis was performed at E35 in cortical sections of control and *ASPM*KO ferrets. **e, f,** Ki67 (e) and TBR2 (f) immunolabeling in cortical sections of control and *ASPM*KO ferrets at E35. **e', f', g,** Distribution of Ki67$^+$ (e'), TBR2$^+$ (f') and TBR2$^+$Ki67$^+$ (g) cells in the cortex of control and *ASPM*KO ferrets (TBR2 and TBR2$^+$Ki67$^+$: n=3 CT, n=4 KO ferrets; Ki67: n=3 CT, n=5 KO ferrets; two-way ANOVA – Šídák's multiple comparisons test; Ki67: $F_{9,60}$=4.772; TBR2: $F_{9,50}$=5.233; TBR2$^+$Ki67$^+$: $F_{9,50}$=3.735). **h,** TBR2$^+$Ki67$^+$ cells in the cortex of control and *ASPM*KO ferrets (n ≥ 3 mice per group; unpaired t-test). Low and top lines represent the limits of the VZ and CP, respectively. Values are mean ± SEM; **p*<0.05, ***p*<0.01, ***p<0.001. Scale bar: 50 µm.